

Chasing Puppies: Mobile Beacon Routing on Closed Curves

Mikkel Abrahamsen^{*} *Jeff Erickson*[†] *Irina Kostitsyna*[‡] *Maarten Löffler*[§] *Tillmann Miltzow*[§]
Jérôme Urhausen[§] *Jordi Vermeulen*[§] *Giovanni Viglietta*[¶]

1 ABSTRACT. We solve an open problem posed by Michael Biro at CCCG 2013 that was
2 inspired by his and others' work on beacon-based routing. Consider a human and a puppy
3 on a simple closed curve in the plane. The human can walk along the curve at bounded
4 speed and change direction as desired. The puppy runs along the curve (faster than the
5 human) always reducing the Euclidean straight-line distance to the human, and stopping
6 only when the distance is locally minimal. Assuming that the curve is smooth (with some
7 mild genericity constraints) or a simple polygon, we prove that the human can always catch
8 the puppy in finite time. Our results hold regardless of the relative speeds of puppy and
9 human, and even if the puppy's speed is unbounded.

^{*}*Basic Algorithms Research Copenhagen (BARC), University of Copenhagen, Denmark, miab@di.ku.dk*

[†]*University of Illinois at Urbana-Champaign, USA jeffe@illinois.edu, jeffe@illinois.edu*

[‡]*Eindhoven University of Technology, Netherlands, i.kostitsyna@tue.nl*

[§]*Department of Information and Computing Sciences, Utrecht University, Netherlands,
[m.loffler|t.miltzow|j.e.urhausen|j.l.vermeulen]@uu.nl*

[¶]*Japan Advanced Institute of Science and Technology, Nomi City, Ishikawa, Japan, johnny@jaist.ac.jp*

10 **1 Introduction**

11 You have lost your puppy somewhere on a simple closed curve. Both of you are forced to
 12 stay on the curve. You can see each other and both want to reunite. The problem is that the
 13 puppy runs faster than you, and it believes naively that it is always a good idea to minimize
 14 its straight-line distance to you. What do you do?

15 To be more precise, let $\gamma: S^1 \hookrightarrow \mathbb{R}^2$ be a simple closed curve in the plane, which we
 16 informally call the *track*. Two special points move around the track, called the *puppy* p and
 17 the *human* h . The human can walk along the track at bounded speed and change direction
 18 as desired. The puppy runs with unbounded speed along the track as long as its Euclidean
 19 straight-line distance to the human is decreasing, until it reaches a point on the curve where
 20 the distance is locally minimized. As the human moves along the track, the puppy moves
 21 to stay at a local distance minimum. The human's goal is to move in such a way that the
 22 puppy and the human meet. See Figure 1 for a simple example.

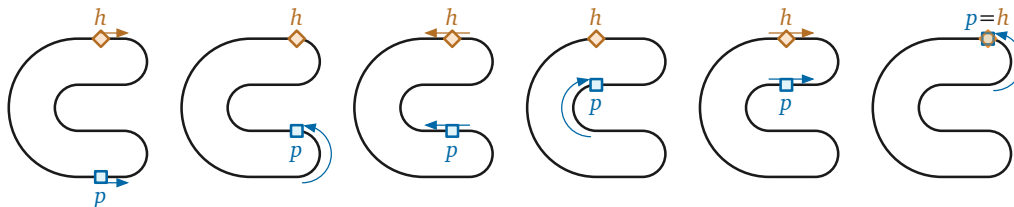


Figure 1: Catching the puppy.

23 In this paper we show that it is always possible to reunite with the puppy under the
 24 assumption that the curve is well-behaved (in a sense to be defined), or if the curve is a
 25 polygon. From this result it easily follows that catching a puppy that moves at any bounded
 26 speed is also possible: the strategy is essentially the same as for the unbounded-speed case,
 27 except that the human may have to move at a lower speed or occasionally stop, in order to
 28 let the puppy reach a point of minimal distance before continuing.

29 The problem was posed in a different guise at the open problem session of the 25th
 30 Canadian Conference on Computational Geometry (CCCG 2013) by Michael Biro. In Biro's
 31 formulation, the track was a railway, the human a locomotive, and the puppy a train carriage
 32 that was attracted to an infinitely strong magnet installed in the locomotive.

33 Returning to our formulation of catching a puppy, it was also asked if the human
 34 will always catch the puppy by choosing an arbitrary direction and walking only in that
 35 direction. This turns out not to be the case; consider the star-shaped track in Figure 2.
 36 Suppose the human and puppy start at points h_1 and p_1 , respectively, and the human walks
 37 counterclockwise around the track. When the human reaches h_2 , the puppy runs from p_2
 38 to p'_2 . When the human reaches h_3 , the puppy runs from p_3 to p'_3 . Then the pattern repeats
 39 indefinitely. Examples of this type, where the human walking in the wrong direction will
 40 never catch the puppy, were independently discovered during the conference by some of the
 41 authors and by David Eppstein.

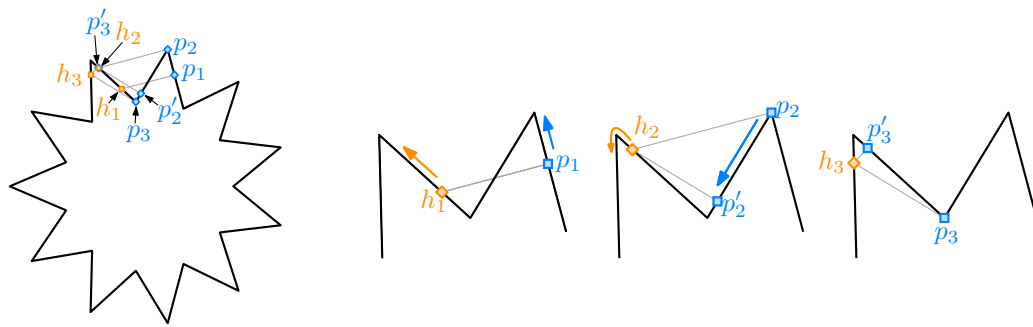


Figure 2: If the human keeps walking counterclockwise from h_1 , the human and the puppy will never meet. To the right are closeups of two of the spikes of the star.

42 1.1 Related work

43 Biro’s problem was inspired by his and others’ work on *beacon-based geometric routing*, a
 44 generalization of both greedy geometric routing and the art gallery problem introduced at
 45 the 2011 Fall Workshop on Computational Geometry [7] and the 2012 Young Researchers
 46 Forum [8], and further developed in Biro’s PhD thesis [6] and papers [9, 10]. A *beacon* is
 47 a stationary point object that can be activated to create a “magnetic pull” towards itself
 48 everywhere in a given polygonal domain P . When a beacon at point b is *activated*, a point
 49 object p moves greedily to decrease its Euclidean distance to b , alternately moving
 50 through the interior of P and sliding along its boundary, until it either reaches b or gets stuck
 51 at a “dead point” where Euclidean distance is minimized. By activating different beacons one
 52 at a time, one can route a moving point object through the domain. Initial results for this
 53 model by Biro and his colleagues [6–10] sparked significant interest and subsequent work in
 54 the community [2, 3, 5, 13, 18, 20–22, 26]. More recent works have also studied how to utilize
 55 objects that repel points instead of attracting them [11, 24].

56 Biro’s problem can also be viewed as a novel variant of classical *pursuit* problems,
 57 which have been an object of intense study for centuries [25]. The oldest pursuit problems ask
 58 for a description of the *pursuit curve* traced by a *pursuer* moving at constant speed directly
 59 toward a *target* moving along some other curve. Pursuit curves were first systematically
 60 studied by Bouguer [12] and de Maupertuis [14] in 1732, who used the metaphor of a pirate
 61 overtaking a merchant ship; another notable example is Hathaway’s problem [16], which asks
 62 for the pursuit curve of a dog swimming at unit speed in a circular lake directly toward a duck
 63 swimming at unit speed around its circumference. In more modern *pursuit-evasion* problems,
 64 starting with Rado’s famous “lion and man” problem [23, pp.114–117], the pursuer and target
 65 both move strategically within some geometric domain; the pursuer attempts to *capture*
 66 the target by making their positions coincide while the target attempts to evade capture.
 67 Countless variants of pursuit-evasion problems have been studied, with multiple pursuers
 68 and/or targets, different classes of domains, various constraints on motion or visibility,
 69 different capture conditions, and so on. Biro’s problem can be naturally described as a
 70 *cooperative pursuit* or *pursuit-attraction* problem, in which a strategic target (the human)
 71 *wants* to be captured by a greedy pursuer (the puppy).

72 Kouhestani and Rappaport [19] studied a natural variant of Biro’s problem, which we
73 can recast as follows. A *guppy* is restricted to a closed and simply-connected *lake*, while the
74 human is restricted to the boundary of the lake. The guppy swims with unbounded speed
75 to decrease its Euclidean distance to the human. Kouhestani and Rappaport described a
76 polynomial-time algorithm that finds a strategy for the human to catch the guppy, if such
77 a strategy exists, given a simple polygon as input; they also conjectured that a capturing
78 strategy always exists. Abel, Akitaya, Demaine, Demaine, Hesterberg, Korman, Ku, and
79 Lynch [1] recently proved that for some polygons and starting configurations, the human
80 cannot catch the guppy, even if the human is allowed to walk in the exterior of the polygon,
81 thereby disproving Kouhestani and Rappaport’s conjecture. Their simplest counterexample
82 is an orthogonal polygon with about 50 vertices.

83 1.2 Our results

84 Before describing our results in detail, we need to carefully define the terms of the problem.
85 The *track* is a simple closed curve $\gamma: S^1 \hookrightarrow \mathbb{R}^2$. We consider the motion of two points on this
86 curve, called the *human* (or *beacon* or *target*) and the *puppy* (or *pursuer*). A *configuration*
87 is a pair $(x, y) \in S^1 \times S^1$ that specifies the locations $h = \gamma(x)$ and $p = \gamma(y)$ for the human
88 and puppy, respectively. Let $D(x, y)$ denote the straight-line Euclidean distance between
89 these two points. When the human is located at $h = \gamma(x)$, the puppy moves from $p = \gamma(y)$
90 to greedily decrease its distance to the human, as follows.

- 91 • If $D(x, y + \varepsilon) < D(x, y)$ for all sufficiently small $\varepsilon > 0$, the puppy runs forward along
92 the track, by increasing the parameter y .
- 93 • If $D(x, y - \varepsilon) < D(x, y)$ for all sufficiently small $\varepsilon > 0$, the puppy runs backward along
94 the track, by decreasing the parameter y .

95 If both of these conditions hold, the puppy runs in an arbitrary direction. While the puppy
96 is running, the human remains stationary. If neither condition holds, the configuration is
97 *stable*; the puppy does not move until the human does. When the configuration is stable,
98 the human can walk in either direction along the track; the puppy walks along the track in
99 response to keep the configuration stable, until it is forced to run again. The human’s goal is
100 to *catch* the puppy; that is, to reach a configuration in which the two points coincide.

101 Our main result is that the human can always catch the puppy in finite time, starting
102 from any initial configuration, provided the track is either a generic simple smooth curve or
103 an arbitrary simple polygon.

104 The remainder of the paper is structured as follows. We begin in Section 2 by
105 considering some variants and special cases of the problem. In particular, we give a simple
106 self-contained proof of our main result for the special case of orthogonal polygons.

107 We consider generic smooth tracks in Sections 3 and 4. Specifically, in Section 3 we
108 define two important diagrams, which we call the *attraction diagram* and the *dual attraction*
109 *diagram*, and prove some useful structural results. At a high level, the attraction diagram is a
110 decomposition of the configuration space $S^1 \times S^1$ according to the puppy’s behavior, similar

111 to the *free space diagrams* introduced by Alt and Godau to compute Fréchet distance [4].
112 We show that for a sufficiently generic smooth track, the attraction diagram consists of a
113 finite number of disjoint simple closed *critical* curves, exactly two of which are topologically
114 nontrivial. Then in Section 4, we argue that the human can catch the puppy on any track
115 whose attraction diagram has this structure.

116 In Section 5, we describe an extension of our analysis from smooth curves to simple
117 polygonal tracks. Because polygons do not have well-defined tangent directions at their
118 vertices, this extension requires explicitly modeling the puppy’s direction of motion in addition
119 to its location. We first prove that the human can catch the puppy on a polygon that has no
120 acute vertex angles and where no three vertices form a right angle; under these conditions,
121 the attraction diagram has exactly the same structure as for generic smooth curves. We then
122 reduce the problem for arbitrary simple polygons to this special case by *chamfering*—cutting
123 off a small triangle at each vertex—and arguing that any strategy for catching the puppy on
124 the chamfered track can be pulled back to the original polygon.

125 Finally, we close the paper by suggesting several directions for further research.

126 Open-source software demonstrating several of the tools developed in this paper
127 is available at <https://github.com/viglietta/Chasing-Puppies> or [https://archive.
128 softwareheritage.org/swh:1:dir:58dd270b0896aa11024666b5cbd2481068e8eab9](https://archive.softwareheritage.org/swh:1:dir:58dd270b0896aa11024666b5cbd2481068e8eab9) .

129 2 Warmup: other settings and a special case

130 In this section, we discuss two variants of Biro’s problem and the special case of orthogonal
131 polygons.

132 In the first variant, both the human h and the puppy p are allowed to move anywhere
133 in the interior and on the boundary of a simple polygon P . Here, as in beacon routing
134 and Kouhestani and Rappaport’s variant [1, 19], the puppy moves greedily to decrease its
135 Euclidean distance to the human, alternately moving through the interior of P and sliding
136 along its boundary.

137 As we will show in Theorem 1, h has a simple strategy to catch p in this setting,
138 essentially by walking along the dual graph of any triangulation. This is an interesting
139 contrast to the proof by Abel et al. [1] that h and p cannot always meet when h is restricted
140 to the *exterior* of P and p to the interior. Our main result that h and p can meet when both
141 are restricted to the *boundary* of P (even for a much wider class of simple closed curves),
142 somehow sits in between these other two variants.

143 When both h and p are restricted to the interior of P , we propose the following
144 strategy for h ; see Figure 3. Let \mathcal{T} be a triangulation of P and let t_1, \dots, t_k be the path of
145 pairwise adjacent triangles in \mathcal{T} such that $h \in t_1$ and $p \in t_k$. Let e_i be the common edge
146 of t_i and t_{i+1} and let d_i be the midpoint of e_i . Let $\pi = hd_1d_2 \dots d_{k-1}$ be a path from h to
147 d_{k-1} , which is contained in the triangles t_1, \dots, t_{k-1} . The human starts walking along π . As
148 soon as the puppy enters a new triangle, the human recomputes π as described and follows
149 the new path.

150 **Theorem 1.** *The proposed strategy will make h and p meet.*

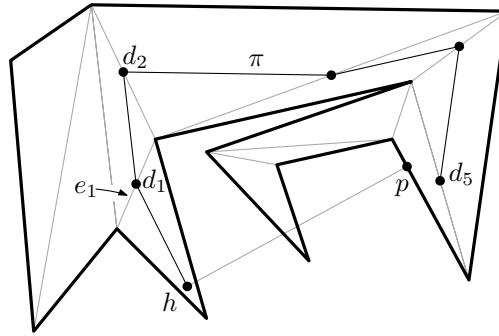


Figure 3: The proposed strategy when h and p are restricted to the interior of a simple polygon P . The human h will follow the path π . Note that the triangle containing p will change before h reaches d_1 , and π will be updated accordingly.

151 *Proof.* First, we observe that if the puppy ever enters the triangle t_1 that is occupied by the
 152 human, then the puppy and the human will meet immediately. Assume that the human does
 153 not meet the puppy right from the beginning. The region $P \setminus t_1$ consists of one, two, or three
 154 polygons, one of which P_p contains p . Thus, whenever the human moves from one triangle
 155 to another, the set of triangles that can possibly contain p shrinks. We conclude that the
 156 human and the puppy must meet eventually. \square

157 In our second variant, the human and the puppy are both restricted to a simple,
 158 closed curve γ in \mathbb{R}^3 . Here it is easy to construct curves on which h and p will never meet;
 159 the simplest example is a “double loop” that approximately winds twice around a planar
 160 circle, as shown in Figure 4.

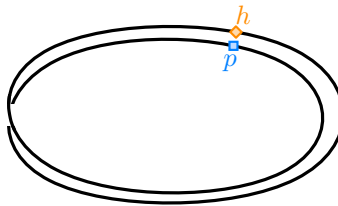


Figure 4: A double loop in \mathbb{R}^3 ; the human and puppy will never meet.

161 Finally, we consider the special case of Biro’s original problem where the track γ is
 162 the boundary of an orthogonal polygon in the plane. This special case of our main results
 163 admits a much simpler self-contained proof.

164 **Theorem 2.** *The human can catch the puppy on any simple orthogonal polygon, by walking*
 165 *counterclockwise around the polygon at most twice.*

166 *Proof.* Let P be an arbitrary simple orthogonal polygon. Let u_1 be its leftmost point with
 167 the maximum y -coordinate, and u_2 be the next boundary vertex of P in the clockwise order
 168 (see Figure 5). Finally, let ℓ be the horizontal line supporting the segment u_1u_2 .

169 We break the motion of the human into two phases. In the first phase, the human
 170 moves counterclockwise around P from the starting location to u_1 . If the human catches the
 171 puppy during this phase, we are done, so assume otherwise. In the second phase, the human
 172 walks counterclockwise around P starting from u_1 to u_2 .

173 We claim that the puppy p is never in the interior of the segment u_1u_2 during the
 174 second phase; thus, p always lies on the closed counterclockwise subpath of P from h to u_2
 175 (or less formally, “between h and u_2 ”). This claim implies that the human and the puppy are
 176 united during the second phase.

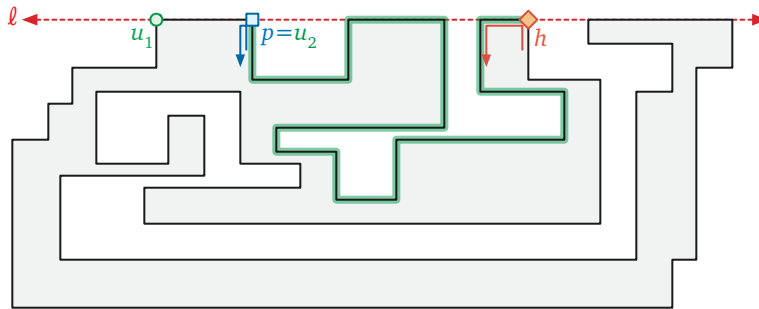


Figure 5: Proof of Theorem 2. During the human’s second trip around P , the puppy lies between u_2 and the human.

177 The puppy must first cross the point u_2 if it ever enters the interior of u_1u_2 . So
 178 consider any moment during the second phase when p moves upward to the vertex u_2 . At
 179 that moment, h must be on the line ℓ to the right of p . (For any point a below ℓ , there is a
 180 point b on the segment below u_2 that is closer to a than u_2 .) Thus, the puppy will stay on
 181 u_2 as long as h is on ℓ . As soon as h leaves ℓ the puppy will leave u_2 downward. Thus the
 182 puppy can never go to the interior of the edge u_1u_2 . \square

183 The star-shaped track in Figure 2 shows that this simple argument does not extend
 184 to arbitrary polygons, even with a constant number of edge directions.

185 3 Diagrams of smooth tracks

186 We first formalize both the problem and our solution under the assumption that the track
 187 is a generic smooth simple closed curve $\gamma: S^1 \hookrightarrow \mathbb{R}^2$. In particular, for ease of exposition,
 188 we assume that γ is regular and C^3 , meaning it has well-defined continuous first, second,
 189 and third derivatives, and its first derivative is nowhere zero. We also assume γ satisfies
 190 some additional genericity constraints, to be specified later. We consider polygonal tracks in
 191 Section 5.

192 3.1 Configurations and genericity assumptions

193 We analyze the behavior of the puppy in terms of the *configuration space* $S^1 \times S^1$, which
 194 is the standard torus. Each configuration point $(x, y) \in S^1 \times S^1$ corresponds to the human

195 being located at $h = \gamma(x)$ and the puppy being located at $p = \gamma(y)$.

196 For any configuration (x, y) , recall that $D(x, y)$ denotes the straight-line Euclidean
 197 distance between the points $\gamma(x)$ and $\gamma(y)$. We classify all configurations $(x, y) \in S^1 \times S^1$
 198 into three types, according to the sign of the partial derivative of distance with respect to
 199 the puppy's position.

- 200 • (x, y) is a *forward* configuration if $\frac{\partial}{\partial y} D(x, y) < 0$.
- 201 • (x, y) is a *backward* configuration if $\frac{\partial}{\partial y} D(x, y) > 0$.
- 202 • (x, y) is a *critical* configuration if $\frac{\partial}{\partial y} D(x, y) = 0$.

203 Starting in any forward (resp. backward) configuration, the puppy automatically runs forward
 204 (resp. backward) along the track γ . Genericity implies that there are a finite number of
 205 critical configurations (x, y) with any fixed value of x , or with any fixed value of y . We
 206 further classify the critical configurations as follows:

- 207 • (x, y) is a *stable* critical configuration if $\frac{\partial^2}{\partial y^2} D(x, y) > 0$.
- 208 • (x, y) is an *unstable* critical configuration if $\frac{\partial^2}{\partial y^2} D(x, y) < 0$.
- 209 • (x, y) is a *forward pivot* configuration if $\frac{\partial^2}{\partial y^2} D(x, y) = 0$ and $\frac{\partial^3}{\partial y^3} D(x, y) < 0$.
- 210 • (x, y) is a *backward pivot* configuration if $\frac{\partial^2}{\partial y^2} D(x, y) = 0$ and $\frac{\partial^3}{\partial y^3} D(x, y) > 0$.

211 In any stable configuration, the puppy's distance to the human is locally minimized, so the
 212 puppy does not move unless the human moves. In any unstable configuration, the puppy can
 213 decrease its distance by running in either direction. Finally, in any forward (resp. backward)
 214 pivot configuration, the puppy can decrease its distance by moving in one direction but not
 215 the other, and thus automatically runs forward (resp. backward) along the track.

216 Critical points can also be characterized geometrically as follows. Refer to Figure 6.
 217 A configuration (x, y) is critical if the human $\gamma(x)$ lies on the line $N(y)$ normal to γ at the
 218 puppy's location $\gamma(y)$. Let $C(y)$ denote the center of curvature of the track at $\gamma(y)$. Then
 219 (x, y) is a pivot configuration if $\gamma(x) = C(y)$, a stable critical configuration if the open ray
 220 from $C(y)$ through the human point $\gamma(x)$ contains the puppy point $\gamma(y)$, and an unstable
 221 critical configuration otherwise.

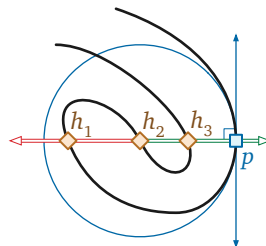


Figure 6: Three critical configurations: (h_1, p) is unstable; (h_2, p) is a pivot configuration, and (h_3, p) is stable.

222 Genericity of the track γ implies that this classification of critical configurations
 223 is exhaustive, and moreover, that the set of pivot configurations is finite. In particular,
 224 our analysis requires that in any pivot configuration (x, y) , the puppy point $\gamma(y)$ is not a
 225 local curvature minimum or maximum.¹ Otherwise, we would need higher derivatives to
 226 disambiguate the puppy's behavior. In the extreme case where γ contains both an open
 227 circular arc α and its center c , all configurations where $h = c$ and $p \in \alpha$ are stable.

228 3.2 Attraction diagrams

229 The *attraction diagram* of the track γ is a decomposition of the configuration space
 230 $S^1 \times S^1$ by critical configurations. Our genericity assumptions imply that the set of critical
 231 points—the common boundary of the forward and backward configurations—is the union of
 232 a finite number of disjoint simple closed curves, which we call *critical cycles*. At least one of
 233 these critical cycles, the main diagonal $x = y$, consists entirely of stable configurations; critical
 234 cycles can also consist entirely of unstable configurations. If a critical cycle is neither entirely
 235 stable nor entirely unstable, then its points of vertical tangency are pivot configurations, and
 236 these points subdivide the curve into x -monotone paths, which alternately consist of stable
 237 and unstable configurations.

238 Figure 7 shows a sketch of the attraction diagram of a simple closed curve. We
 239 visualize the configuration torus $S^1 \times S^1$ as a square with opposite sides identified. Green
 240 and red paths indicate stable and unstable configurations, respectively; blue dots indicate
 241 pivot configurations; and backward configurations are shaded light gray. Figure 8 shows
 242 the attraction diagram for a more complex polygonal track, with slightly different coloring
 243 conventions. (Again, we will discuss polygonal tracks in more detail in Section 5.)

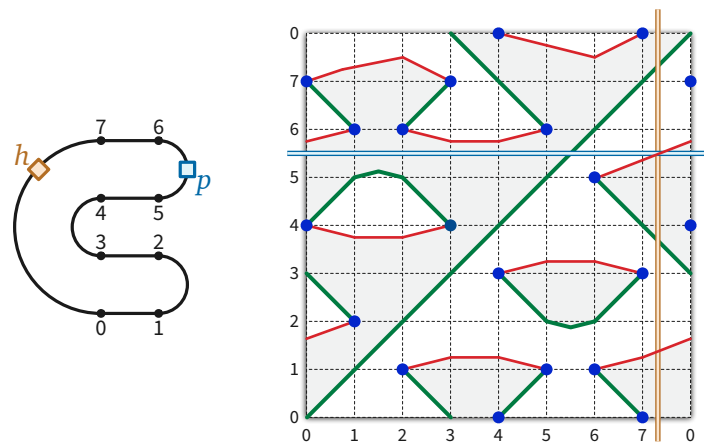


Figure 7: The attraction diagram of a simple closed curve, with one unstable critical configuration emphasized.

244 The cycles in any attraction diagram have a simple but important topological structure.
 245 A critical cycle in the attraction diagram is *contractible* if it is the boundary of a simply

¹More concretely, we assume the track γ intersects its evolute (the locus of centers of curvature) transversely, away from its cusps.

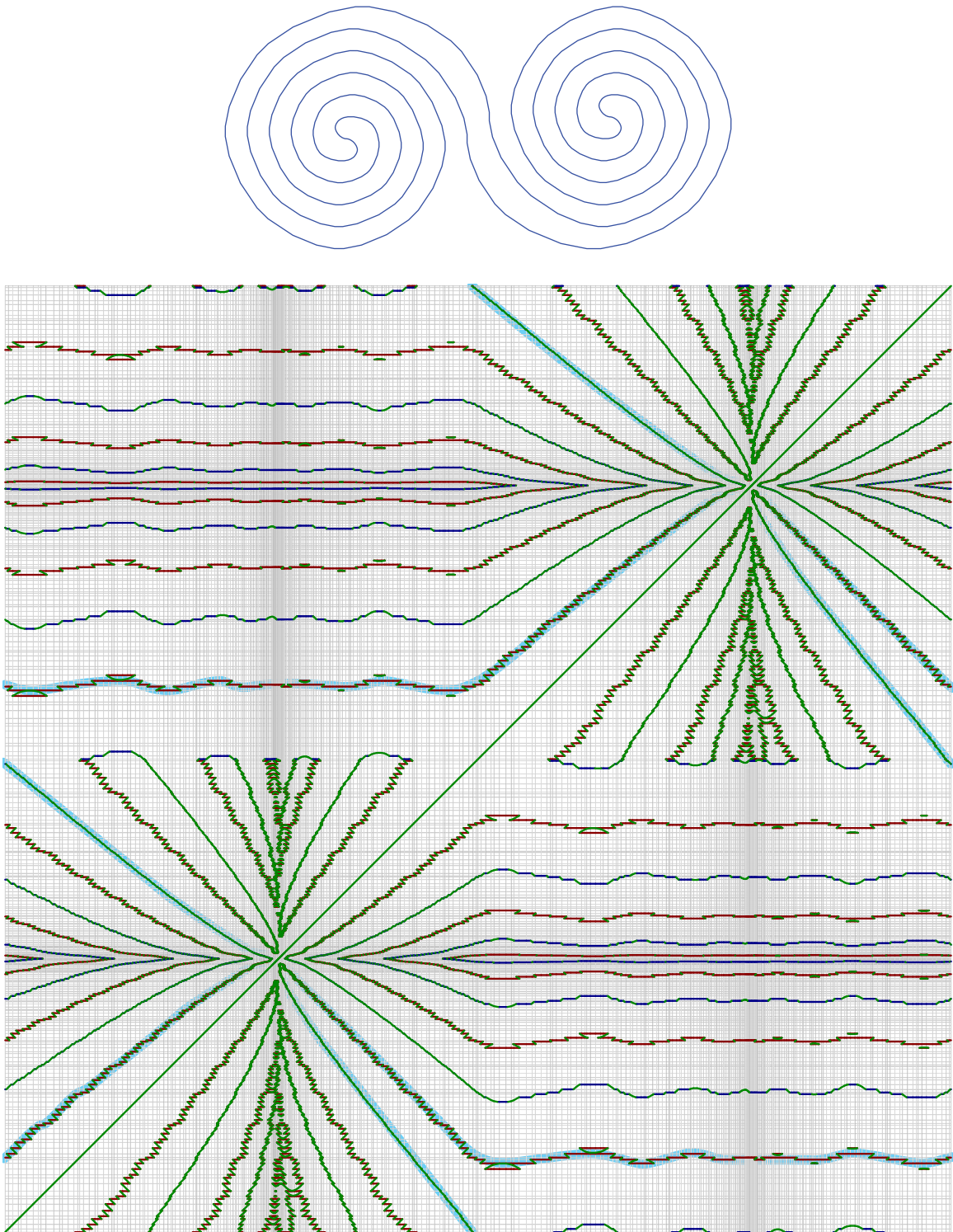


Figure 8: The attraction diagram of a complex simple polygon. Serrations in the diagram are artifacts of the curve being polygonal instead of smooth. The river is highlighted in blue.

246 connected subset of the torus $S^1 \times S^1$ and *essential* otherwise. For example, the main
 247 diagonal is essential, and the attraction diagram in Figure 7 contains two contractible critical
 248 cycles and two essential critical cycles.

249 **Lemma 3.** *The attraction diagram of any generic closed curve contains an even number of*
 250 *essential critical cycles.*

251 *Proof.* This lemma follows immediately from standard homological arguments, but for the
 252 sake of completeness we sketch a self-contained proof.

253 Fix a generic closed curve γ . Let α and β denote the horizontal and vertical cycles
 254 $S^1 \times \{0\}$ and $\{0\} \times S^1$, respectively. Without loss of generality, assume α and β intersect
 255 every critical cycle in the attraction diagram of γ transversely.

256 A critical cycle C in the attraction diagram is contractible if and only if α and β
 257 each cross C an even number of times. (Indeed, this parity condition characterizes all simple
 258 contractible closed curves in the torus.) On the other hand, α and β each cross the main
 259 diagonal once. It follows that α and β each cross *every* essential critical cycle an odd number
 260 of times; otherwise, some pair of essential critical cycles would intersect.

261 Because the critical cycles are the boundary between the forward and backward
 262 configurations, α and β each contain an even number of critical points. The lemma now
 263 follows immediately. \square

264 We emphasize that this lemma does *not* actually require the track γ to be simple;
 265 the argument relies only on properties of generic functions over the torus that are minimized
 266 along the main diagonal.

267 3.3 Dual attraction diagrams

268 Our analysis also relies on a second diagram, which we call the *dual attraction diagram*
 269 of the track. We hope the following intuition is helpful. While the attraction diagram tells
 270 us the possible positions of the puppy depending on the position of the human, the dual
 271 attraction diagram gives us the possible positions of the human depending on the position of
 272 the puppy. For each puppy configuration $y \in S^1$, we consider the normal line $N(y)$. We are
 273 interested in the intersection points of γ with $N(y)$, as those are the possible positions of the
 274 human. The idea of the dual attraction diagram is to trace the positions of the human as a
 275 function of the position of the puppy, see Figure 10.

276 Let $T(y)$ denote the directed line tangent to γ at the point $\gamma(y)$. For any configuration
 277 (x, y) , let $\ell(x, y)$ denote the distance from $\gamma(x)$ to the tangent line $T(y)$, signed so that
 278 $\ell(x, y) > 0$ if the human point $\gamma(x)$ lies to the left of $T(y)$ and $\ell(x, y) < 0$ if $\gamma(y)$ lies to
 279 the right of $T(y)$. More concisely, assuming without loss of generality that the track γ is
 280 parameterized by arc length, $\ell(x, y)$ is twice the signed area of the triangle with vertices
 281 $\gamma(x)$, $\gamma(y)$, and $\gamma(y) + \gamma'(y)$.

282 Let $L: S^1 \times S^1 \rightarrow S^1 \times \mathbb{R}$ denote the function $L(x, y) = (y, \ell(x, y))$. The dual
 283 attraction diagram is the decomposition of the infinite cylinder $S^1 \times \mathbb{R}$ by the points

284 $\{L(x, y) \mid (x, y) \text{ is critical}\}$. At the risk of confusing the reader, we refer to the image
 285 $L(x, y) \in S^1 \times \mathbb{R}$ of any critical configuration (x, y) as a critical point of the dual attraction
 286 diagram.

287 The dual attraction diagram can also be described as follows. For any $y \in S^1$
 288 and $d \in \mathbb{R}$, let $\Gamma(y, d)$ denote the point on the normal line $N(y)$ at distance d to the left
 289 of the tangent vector $\gamma'(y)$. More formally, assuming without loss of generality that γ
 290 is parameterized by arc length, we have $\Gamma(y, d) = \gamma(y) + d \begin{bmatrix} 0 & -1 \\ 1 & 0 \end{bmatrix} \gamma'(y)$. We emphasize
 291 that $\Gamma(y, d)$ does not necessarily lie on the curve γ . The dual attraction diagram is the
 292 decomposition of the cylinder $S^1 \times \mathbb{R}$ by the preimage $\Gamma^{-1}(\gamma)$ of γ .

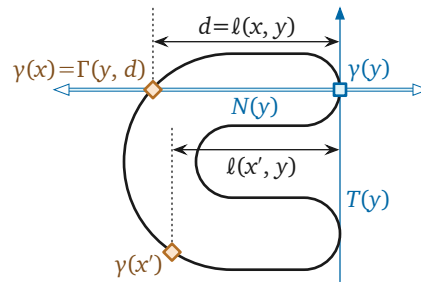


Figure 9: Examples of the functions l and Γ used to define the dual attraction diagram.

293 Because γ is simple and regular, the dual attraction diagram is the union of simple
 294 disjoint closed curves. The function L continuously maps each critical cycle in the attraction
 295 diagram to a closed curve in the cylinder $S^1 \times \mathbb{R}$; we also call this image curve a *critical cycle*.
 296 Thus, the restriction of L to the set of critical configurations is a homeomorphism onto its
 297 image in the dual attraction diagram. In particular, L maps the main diagonal $x = y$ to the
 298 horizontal axis $l(x, y) = 0$ of the dual attraction diagram. We emphasize, however, that the
 299 two diagrams are not topologically equivalent. Figure 10 shows the dual attraction diagram
 300 of the same track whose attraction diagram is shown in Figure 7; here preimages of points
 301 inside the track are shaded.

302 Just as in the attraction diagram, a critical cycle in the dual attraction diagram is
 303 *contractible* if it is the boundary of a simply connected subset of the cylinder $S^1 \times \mathbb{R}$ and
 304 *essential* otherwise.

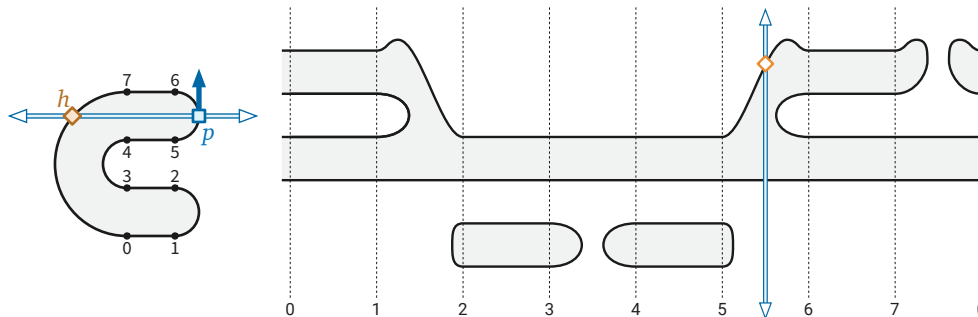


Figure 10: The dual attraction diagram of a simple closed curve, with one critical configuration emphasized. Compare with Figure 7.

305 **Lemma 4.** *The function L bijectively maps essential critical cycles in the attraction diagram*
 306 *to essential critical cycles in the dual attraction diagram. In particular, the two diagrams*
 307 *have the same number of essential critical cycles.*

308 *Proof.* Let $\alpha = S^1 \times \{0\}$ and $\alpha' = S^1 \times \{0\}$ denote the horizontal cycles in the torus $S^1 \times S^1$
 309 and in the infinite cylinder $S^1 \times \mathbb{R}$, respectively. Let C be any critical cycle on the attraction
 310 diagram, and let $C' = L(C)$ be the corresponding critical cycle in the dual attraction diagram.

311 Recall from the proof of Lemma 3 that C is contractible on the torus if and only if
 312 $|C \cap \alpha|$ is even. Similarly, C' is contractible in the cylinder if and only if $|C' \cap \alpha'|$ is even.
 313 The map $L: S^1 \times S^1 \rightarrow S^1 \times \mathbb{R}$ maps $C \cap \alpha$ bijectively to $C' \cap \alpha'$. We conclude that C is
 314 essential if and only if C' is essential. \square

315 With this correspondence in hand, we can now more carefully describe the topological
 316 structure of the *attraction* diagram when the track is simple.

317 **Lemma 5.** *The attraction diagram of a **simple** generic closed curve contains **exactly two***
 318 *essential critical cycles.*

319 *Proof.* Fix a generic closed curve γ . Lemma 3 implies that the attraction diagram of γ
 320 contains at least two essential critical cycles, one of which is the main diagonal. Thus, to
 321 prove the lemma, it remains to show that there are *at most* two essential critical cycles, in
 322 either the attraction diagram or the dual attraction diagram.

323 Let $\Sigma \subset S^1 \times \mathbb{R}$ denote the set of essential critical cycles in the *dual attraction*
 324 diagram. Any two cycles in Σ are homotopic—meaning one can be continuously deformed
 325 into the other—because there is only one nontrivial homotopy class of simple cycles on the
 326 infinite cylinder $S^1 \times \mathbb{R}$. It follows that the cycles in Σ have a well-defined vertical total
 327 order. In particular, the highest and lowest intersection points between any vertical line
 328 and Σ always lie on the *same* two essential cycles in Σ .

329 Without loss of generality, suppose $\gamma(0)$ is a point on the boundary of the convex hull
 330 of γ . Let C be any essential critical cycle in the attraction diagram of γ , and let $C' = L(C)$
 331 denote the corresponding essential cycle in the dual attraction diagram. The cycle C must
 332 pass through all possible puppy positions *and* all possible human positions; thus, C contains
 333 a configuration $(0, y)$ for some parameter $y \in S^1$. Recall that $N(y)$ denotes the line normal
 334 to γ at $\gamma(y)$. Then $\gamma(0)$ must be an endpoint of the convex hull of $\gamma \cap N(y)$, which is a line
 335 segment. We conclude that C' must be either the highest or lowest essential critical cycle in
 336 the dual attraction diagram. Therefore, there are at most two critical cycles, completing the
 337 proof. \square

338 In the rest of the paper, we mnemonically refer to the two essential critical cycles in
 339 the attraction diagram of a simple track as the *main diagonal* and the *river*.

340 We emphasize that the converse of Lemma 5 is false; there are non-simple tracks
 341 whose attraction diagrams have exactly two essential critical cycles. (Consider the figure-eight
 342 curve ∞ .) Moreover, we conjecture that Lemma 5 can be generalized to all (smooth) tracks
 343 with turning number ± 1 .

344 **4 Dexter and sinister strategies**

345 We can visualize any strategy for the human to catch the puppy as a path through the
 346 attraction diagram, consisting entirely of segments of stable critical paths and vertical
 347 segments, that ends on the main diagonal, as shown in Figure 11. We refer to the vertical
 348 segments as *pivots*. Every pivot (except possibly the first) starts at a pivot configuration,
 349 and every pivot ends at a stable configuration.

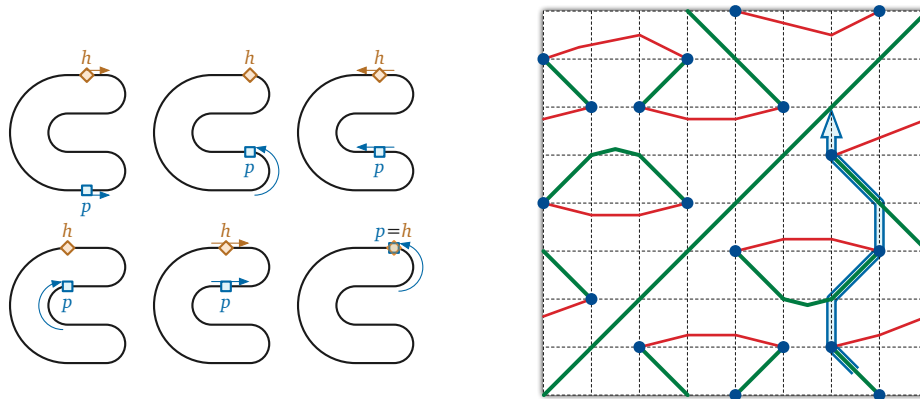


Figure 11: A sinister strategy for catching the puppy; compare with Figures 1 and 7.

350 We call a strategy **dexter** if it ends with a backward pivot—a *downward* segment,
 351 approaching the main diagonal to the *right*—and we call a configuration (x, y) *dexter* if
 352 there is a dexter strategy for catching the puppy starting at (x, y) . Similarly, a strategy is
 353 **sinister** if it ends with a forward pivot—a *skyward* segment, approaching the main diagonal
 354 to the *left*—and a configuration is sinister if it is the start of a sinister strategy.² A single
 355 configuration can be both dexter and sinister; see Figure 12.

356 **Theorem 6.** *Let γ be a generic track whose attraction diagram has exactly two essential*
 357 *critical cycles. Every configuration on γ is dexter or sinister, or possibly both; thus, the*
 358 *human can catch the puppy on γ from any starting configuration.*

359 Before giving the proof, we emphasize that Theorem 6 does not require the track γ
 360 to be simple. Also, it is an open question whether having exactly two essential critical cycle
 361 curves is a *necessary* condition for the human to always be able to catch the puppy. (We
 362 conjecture that it is not.)

363 *Proof.* Fix a generic track γ whose attraction diagram has exactly two essential critical cycles,
 364 which we call the *main diagonal* and the *river*. Assume γ has at least one pivot configuration,
 365 since otherwise, from any starting configuration, the puppy runs directly to the human.

366 Let D be the set of all dexter configurations, and let S be the set of all sinister
 367 configurations. We claim that D and S are both annuli that contain both the main diagonal
 368 and the river. Because S and D meet on opposite sides of the main diagonal, this claim

²*Dexter* and *sinister* are Latin for right (or skillful, or fortunate, or proper, from a Proto-Indo-European root meaning “south”) and left (or unlucky, or unfavorable, or malicious), respectively.

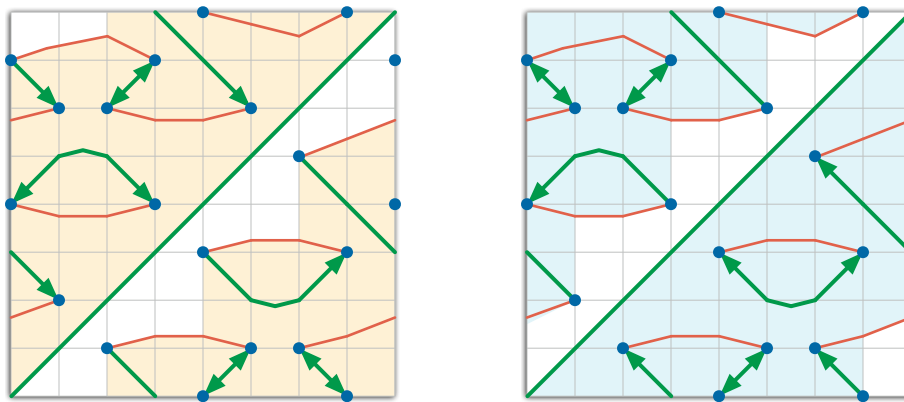


Figure 12: Dexter (orange) and sinister (cyan) configurations in the example attraction diagram. Arrows on the stable critical paths describe dexter and sinister strategies for catching the puppy.

369 implies that $D \cup S$ is the entire torus, completing the proof of the lemma. We prove our
 370 claim explicitly for D ; a symmetric argument establishes the claim for S .

371 For purposes of argument, we partition the attraction diagram of γ by extending
 372 vertical segments from each pivot configuration to the next critical cycles directly above and
 373 below. We call the cells in this decomposition *trapezoids*, even though their top and bottom
 374 boundaries may not be straight line segments. At each forward pivot configuration p , we
 375 color the vertical segment above (x, y) *green* and the vertical segment below p *red*; the colors
 376 are reversed for backward vertical segments, see Figure 13.

377 The first step of any strategy is a (possibly trivial) pivot onto a stable critical path.
 378 Because the human and puppy can move freely within any stable critical path σ , either every
 379 point in σ is dexter, or no point in σ is dexter. Similarly, for any green pivot segment π ,
 380 either every point in π is dexter or no point in π is dexter.

381 Consider any trapezoid τ , and let σ be the stable critical path on its boundary.
 382 Starting in any configuration in τ , the puppy immediately moves to a configuration on σ .
 383 Thus, if any point in τ is dexter, then σ is dexter, which implies that *every* point in τ is
 384 dexter. Thus, we can describe entire trapezoids as dexter or not dexter. It follows that D is
 385 the union of trapezoids.

386 If two trapezoids share a stable critical path *other than the main diagonal*, then either
 387 both trapezoids are dexter or neither is dexter. Similarly, if the green pivot segment leaving
 388 a pivot configuration p is dexter, then all four trapezoids incident to p are dexter; otherwise,
 389 either two or none of these four trapezoids are dexter.

390 We conclude that aside from the main diagonal, the boundary of D consists entirely
 391 of unstable critical paths, pivot configurations, and red vertical segments. Moreover, for
 392 every pivot configuration p on the boundary of D , the green pivot segment leaving p is *not*
 393 dexter.

394 By definition, every point in D is connected by a (dexter) path to the main diagonal,

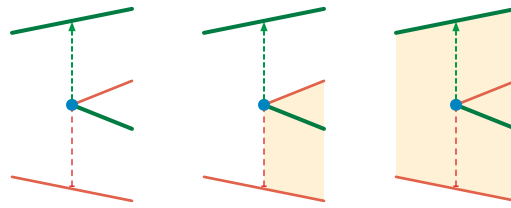


Figure 13: Possible arrangements of dexter trapezoids near a forward pivot configuration.

395 so D is non-empty and connected. On the other hand, D excludes a complete cycle of
 396 forward configurations just below the main diagonal. For any $x \in S^1$, let $D(x)$ denote the
 397 set of dexter configurations (x, y) ; this set consists of one or more vertical line segments in
 398 the attraction diagram.

399 Suppose for the sake of argument that some set $D(x)$ is disconnected. Because D is
 400 connected, the boundary of D must contain a *concave vertical bracket*: A vertical boundary
 401 segment π whose adjacent critical boundary segments both lie (without loss of generality)
 402 to the right of π , but D lies locally to the left of π . See Figure 14. Let p be the pivot
 403 configuration at one end of π . The green vertical segment on the other side of p is dexter,
 404 which implies that *all* trapezoids incident to p are dexter, contradicting the assumption that
 405 π lies on the boundary of D . We conclude that for all x , the set $D(x)$ is a single vertical line
 406 segment; in other words, D is a *monotone* annulus.

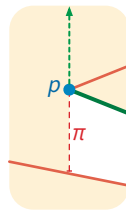


Figure 14: A hypothetical concave vertical bracket on the boundary of D .

407 The bottom boundary of D is the main diagonal. The monotonicity of D implies that
 408 the top boundary of D is a monotone “staircase” alternating between upward red vertical
 409 segments and rightward unstable critical paths. Every trapezoid immediately above the top
 410 boundary of D contains only forward configurations. Thus, there is a complete essential
 411 cycle ϕ of forward configurations just above the upper boundary of D . Because ϕ contains
 412 only forward configurations, ϕ must lie entirely above the river. It follows that D contains
 413 the entire river.

414 Symmetrically, S is an annulus bounded above by the main diagonal and bounded
 415 below by a non-contractible cycle of backward configurations; in particular, the entire river
 416 lies inside S . We conclude that $D \cup S$ is the entire configuration torus. \square

417 If the attraction diagram of γ has more than two essential critical cycles curves, then
 418 D and S are still monotone annuli, each bounded by the main diagonal and an essential
 419 cycle of red vertical segments and unstable paths, and thus S and D each contain at least

420 one essential critical cycle other than the main diagonal. However, $D \cup S$ need not cover the
 421 entire torus.

422 **Corollary 7.** *The human can catch the puppy on any generic simple closed track, from any*
 423 *starting configuration.*

424 5 Polygonal tracks

425 Our previous arguments require, at a minimum, that the track has a continuous derivative
 426 that is never equal to zero. We now extend our results to polygonal tracks, which do not
 427 have well-defined tangent directions at their vertices.

428 5.1 Polygonal attraction diagrams

429 Throughout this section, we fix a simple polygonal track P with n vertices. We regard P as
 430 a continuous piecewise linear function $P: S^1 \hookrightarrow \mathbb{R}^2$, parameterized by arc length. Without
 431 loss of generality $P(0)$ is a vertex of the track. We index the vertices and edges of P in order,
 432 starting with $v_0 = P(0)$, where edge e_i connects v_i to v_{i+1} ; all index arithmetic is implicitly
 433 performed modulo n .

434 To properly describe the puppy's behavior, we must also account for the direction
 435 that the puppy is facing, even when the puppy lies at a vertex. To that end, we represent
 436 the track using both a continuous *position* function $\pi: S^1 \rightarrow \mathbb{R}^2$ and a continuous *direction*
 437 function $\theta: S^1 \rightarrow S^1$. Intuitively, the two functions describe the position and orientation of
 438 the puppy as it makes a complete circuit along P : it advances at constant speed along each
 439 edge, and it stops at each vertex to modify its direction vector, again at constant speed.

440 To be precise, both $\pi(y)$ and $\theta(y)$ are piecewise linear functions of the puppy's
 441 parameter $y \in S^1$. The curve $\pi(y)$ is a re-parameterization of P such that, when $\pi(y)$ is
 442 in the interior of an edge e_i of P , its derivative $\pi'(y)$ is a constant positive multiple of
 443 $\theta(y) = (v_{i+1} - v_i)/\|v_{i+1} - v_i\|$. Moreover, for each vertex v_i of P , the preimage $\pi^{-1}(v_i)$
 444 is a non-degenerate interval $[a_i, b_i] \subset S^1$ such that $\pi'(y) = 0$ whenever $a_i < y < b_i$; also,
 445 $\theta(a_i) = (v_i - v_{i-1})/\|v_i - v_{i-1}\|$, $\theta(b_i) = (v_{i+1} - v_i)/\|v_{i+1} - v_i\|$, and $\theta(y)$ is linear and injective
 446 on $[a_i, b_i]$, turning clockwise if the edges e_{i-1} and e_i define a clockwise turn, and vice versa.
 447 (The ratio of the speeds at which the puppy moves along edges and turns around at vertices
 448 is not relevant.)

449 We classify any human-puppy configuration $(x, y) \in S^1 \times S^1$ as *forward*, *backward*, or
 450 *critical*, if the dot product $(P(x) - \pi(y)) \cdot \theta(y)$ is negative, positive, or zero, respectively. In any
 451 forward configuration (x, y) , the puppy moves to increase the parameter y ; in any backward
 452 configuration, the puppy moves to decrease the parameter y . (The human's direction is
 453 irrelevant.) The *attraction diagram* is the set of all critical configurations $(x, y) \in S^1 \times S^1$.
 454 We further classify critical configurations (x, y) as follows:

- 455 • *final* if $P(x) = \pi(y)$,
- 456 • *stable* if $(x, y - \varepsilon)$ is forward and $(x, y + \varepsilon)$ is backward for all suffic. small $\varepsilon > 0$,

- 457 • *unstable* if $(x, y - \varepsilon)$ is backward and $(x, y + \varepsilon)$ is forward for all suffic. small $\varepsilon > 0$,
 458 • *forward pivot* if $(x, y - \varepsilon)$ and $(x, y + \varepsilon)$ are both forward for all suffic. small $\varepsilon > 0$, or
 459 • *backward pivot* if $(x, y - \varepsilon)$ and $(x, y + \varepsilon)$ are both backward for all suffic. small $\varepsilon > 0$.

460 A straightforward case analysis implies that this classification is exhaustive.

461 To define the attraction diagram of P , we decompose the torus $S^1 \times S^1$ into a $2n \times n$
 462 grid of rectangular cells, where each column corresponds to an edge e_j containing the human,
 463 and each row corresponds to either a vertex v_i or an edge e_i containing the puppy. The *main*
 464 *diagonal* of the attraction diagram is the set of all final configurations. Strictly speaking, in
 465 this case the “main diagonal” is not just a straight line, but consists of alternating diagonal
 466 and vertical segments. We can characterize the critical points inside each cell as follows:

467 Each edge-edge cell $e_i \times e_j$ contains at most one boundary-to-boundary path of stable
 468 critical configurations (x, y) . Refer to Figure 15.

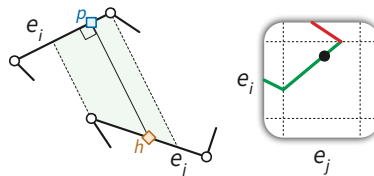


Figure 15: All edge-edge critical configurations are stable.

469 Each vertex-edge cell $v_i \times e_j$ contains at most one boundary-to-boundary path of
 470 stable critical configurations and at most one boundary-to-boundary path of unstable
 471 critical configurations. If the cell contains both paths, they are disjoint. A configuration (x, y) with
 472 $\pi(y) = v_i$ is stable if and only if $P(x)$ lies in the outer normal cone at v_i , and unstable if and
 473 only if $P(x)$ lies in the inner normal cone at v_i ; see Figure 16.

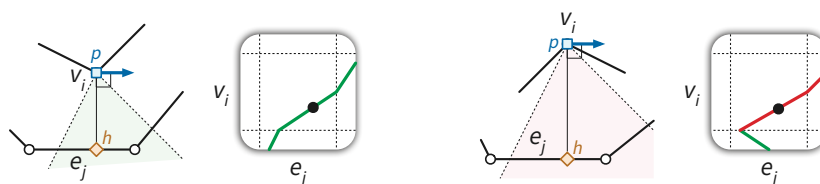


Figure 16: Stable and unstable vertex-edge critical configurations.

474 5.2 Polygonal pivot configurations

475 Unlike the attraction diagrams of generic smooth curves defined in Section 3.2, the attraction
 476 diagrams of polygons are not always well-behaved. In particular, a pivot configuration
 477 may be incident to more (or fewer) than two critical curves, and in extreme cases, pivot
 478 configurations need not even be discrete. We call such a configuration a *degenerate* pivot
 479 configuration.

480 In any pivot configuration (x, y) , the puppy $\pi(y)$ lies at some vertex v_i , the puppy's
 481 direction $\theta(y)$ is parallel to either e_i (or e_{i+1}). Generically, each pivot configuration is a
 482 shared endpoint of an unstable critical path in cell $v_i \times e_j$ and a stable critical path in cell
 483 $e_i \times e_j$ (or $e_{i-1} \times e_j$); see Figure 17.

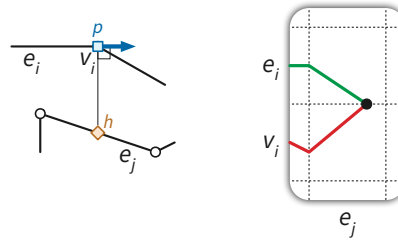


Figure 17: Near a non-degenerate pivot configuration.

484 There are three distinct ways in which degenerate pivot configurations can appear.

485 A **type-1 degeneracy** is caused by an acute angle on P . Specifically, let v_i be a
 486 vertex of P . The configuration (x, y) with $P(x) = \pi(y) = v_i$ is degenerate if the angle
 487 between e_{i-1} and e_i is strictly acute. In the attraction diagram of a type-1 degeneracy, two
 488 stable critical curves and two unstable critical curves end on a single vertical section of the
 489 main diagonal (corresponding to the human and the puppy being both at v_i , but the puppy
 490 facing in different directions). Refer to Figure 18.

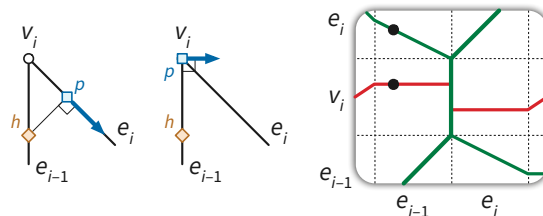


Figure 18: Stable and unstable configurations near an acute vertex angle.

491 A **type-2 degeneracy** is caused by a more specific configuration. Let e_i be an edge
 492 of P , and let ℓ be the line perpendicular to e_i through v_i (or, symmetrically, through v_{i+1}).
 493 Let v_j be another vertex of P which lies on ℓ . The configuration (x, y) with $P(x) = v_j$ and
 494 $\pi(y) = v_i$ is degenerate if:

- 495 • v_{i-1} and v_j lie in the same open halfspace of the supporting line of e_i ; **and**
- 496 • v_{j-1} and v_{j+1} lie in the same open halfspace of ℓ .

497 A type-2 degeneracy corresponds to a vertex (pivot configuration) of degree 4 or 0 in the
 498 attraction diagram. We further distinguish these as *type-2a* and *type-2b*. Refer to Figure 19.

499 Finally, a **type-3 degeneracy** is essentially a limit of both of the previous types of
 500 degeneracies. Let e_i be an edge of P , let ℓ be the line perpendicular to e_i through v_i , and
 501 let e_j be another edge of P which lies on ℓ . The configuration (x, y) with $P(x) \in e_j$ and

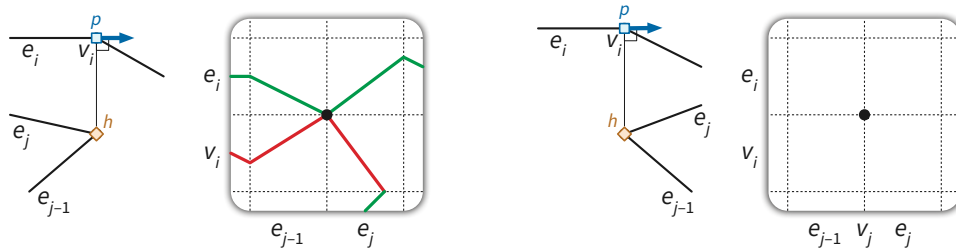


Figure 19: Type-2a and type-2b degenerate pivot configurations.

502 $\pi(y) = v_i$ is degenerate if vertices v_{i-1} and v_j lie in the same open halfspace of the supporting
 503 line of e_i . When this degeneracy occurs, pivot configurations are not discrete, because
 504 the point $P(x) \in e_j$ can be chosen arbitrarily. Moreover, the vertex-vertex configurations
 505 (v_j, v_i) and (v_{j-1}, v_i) have odd degree in the attraction diagram. A type-3 degeneracy can
 506 be connected to (two or more) other critical curves, or be isolated. We further distinguish
 507 these as *type-3a* and *type-3b*, depending on whether v_i is an endpoint of e_j . See Figure 20.

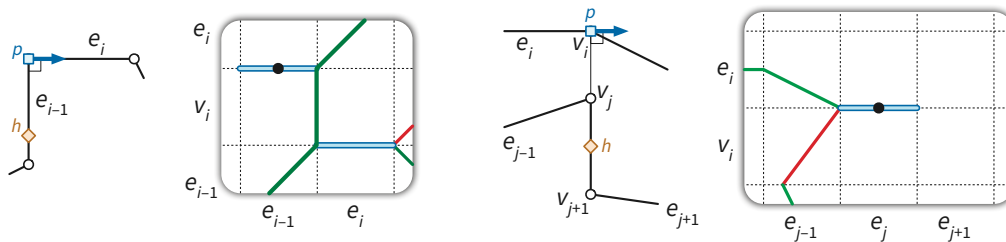


Figure 20: Type-3a and type-3b degenerate pivot configurations.

508 In Section 5.3 we first consider polygonal tracks which do not have any degeneracies
 509 of these three types. To simplify exposition, we forbid degeneracies by assuming that no
 510 vertex angle in P is acute and that no three vertices of P define a right angle. In Section 5.5
 511 we lift these assumptions by *chamfering* the polygon, cutting off a small triangle at each
 512 vertex.

513 5.3 Catching puppies on generic obtuse polygons

514 Generic obtuse polygonal tracks behave almost identically to smooth tracks, once we properly
 515 define the attraction diagram and dual attraction diagram.

516 **Lemma 8.** *Let P be a simple polygon with no acute vertex angles, in which no three vertices*
 517 *define a right angle. The attraction diagram of P is the union of disjoint simple critical*
 518 *cycles.*

519 *Proof.* Each edge-edge cell $e_i \times e_j$ contains at most one section of stable critical configurations
 520 (x, y) (Figure 15). For each such configuration, the points $\pi(y) \in e_i$ and $P(x) \in e_j$ are
 521 connected by a line perpendicular to e_i . Because no three vertices of P define a right angle,

522 these points cannot both be vertices of P ; thus, any critical path inside the cell $e_i \times e_j$ avoids
 523 the corners of that cell.

524 Each vertex-edge cell $v_i \times e_j$ contains at most one section of a stable and one section
 525 of an unstable path (Figure 16). Again, because no three vertices of P define a right angle,
 526 these paths avoid the corners of the cell $v_i \times e_j$.

527 It follows from the definition of pivot that, in any pivot configuration (x, y) , the
 528 puppy lies at a vertex $\pi(y) = v_i$, and the puppy's direction $\theta(y)$ is parallel to either e_i (or
 529 e_{i+1}). Also, by the above, the human lies in the interior of some edge: $P(x) \in e_j$. Moreover,
 530 our assumptions on P imply that there are no degenerate pivot configurations; thus, each
 531 pivot configuration is a shared endpoint of exactly one unstable critical path in cell $v_i \times e_j$
 532 and exactly one stable critical path in cell $e_i \times e_j$ (or $e_{i-1} \times e_j$).

533 Thus, the set of unstable critical configurations is the union of x -monotone paths
 534 whose endpoints are pivot configurations. Similarly, the set of stable critical configurations
 535 is also the union of x -monotone paths whose endpoints are pivot configurations. Moreover,
 536 each unstable critical path lies in a single vertex strip.

537 Because every vertex angle in P is obtuse, every configuration (x, y) where the human
 538 $P(x)$ lies on an edge e_i and the puppy $\pi(y)$ lies on the previous edge e_{i-1} is either forward of
 539 final. Similarly, if $P(x) \in e_{i-1}$ and $\pi(y) \in e_i$, then the configuration (x, y) is either backward
 540 or final. Thus, the main diagonal is disjoint from all other critical cycles; in fact, no other
 541 critical cycle intersects any grid cell that touches the main diagonal.

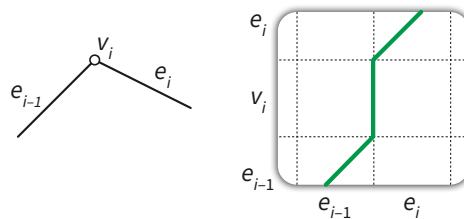


Figure 21: Near the main diagonal.

542 This completes the classification of all critical configurations. We conclude that the
 543 attraction diagram consists of the (simple, closed) main diagonal and possibly other simple
 544 closed curves composed of stable and unstable critical paths meeting at pivot configurations.
 545 All these critical cycles are disjoint. \square

546 **Lemma 9.** *Let P be a simple polygon with no acute vertex angles, in which no three vertices*
 547 *define a right angle. If the attraction diagram of P has exactly two essential critical cycles,*
 548 *then the human can catch the puppy on P , starting from any initial configuration.*

549 The remainder of the proof is essentially unchanged from the smooth case. For any
 550 configuration (x, y) , let $T(y)$ denote the directed “tangent” line through $\pi(y)$ in direction
 551 $\theta(y)$, and let $L(x, y)$ denote the signed distance from $P(x)$ to $T(y)$, signed positively if $P(x)$
 552 lies to the left of $T(y)$ and negatively if $P(x)$ lies to the right of $T(y)$. The *dual attraction*
 553 *diagram* of P consists of all points $(y, L(x, y)) \in S^1 \times \mathbb{R}$ where (x, y) is a critical configuration.

554 As in the smooth case, the map $(x, y) \mapsto (y, L(x, y))$ is a homeomorphism from the critical
 555 cycles in the attraction diagram to the curves in the dual attraction diagram; moreover, this
 556 map preserves the contractibility of each critical cycle.

557 **Lemma 10.** *Let P be a simple polygon with no acute vertex angles, in which no three vertices*
 558 *define a right angle. The attraction diagram of P contains exactly two essential critical cycles.*

559 **Theorem 11.** *Let P be a simple polygon with no acute vertex angles, in which no three*
 560 *vertices define a right angle. The human can catch the puppy on P , starting from any initial*
 561 *configuration.*

562 We can easily extend this theorem to polygons with degenerate pivot configurations
 563 of type 2b and type 3b. Since these correspond to vertically isolated forward or backward
 564 pivot configurations in the attraction diagram, they do not impact the existence of a strategy
 565 to catch the puppy. The puppy will just move over them as if they were normal forward or
 566 backward configurations.

567 **Corollary 12.** *Let P be a simple polygon with no degeneracies of type 1, type 2a, or type 3a.*
 568 *The human can catch the puppy on P , starting from any initial configuration.*

569 5.4 Chamfering

570 We now extend our analysis to arbitrary simple polygons. We define a *chamfering* operation,
 571 which transforms a polygon P into a new polygon \bar{P} . First we show that \bar{P} has no degenerate
 572 pivot configurations of type 1, 2a, or 3a (although it may still have degeneracies of type 2b
 573 and type 3b). Hence there is a strategy to catch the puppy on \bar{P} . Finally, we show that such
 574 a strategy can be correctly translated back to a strategy on P .

575 Let P be an arbitrary simple polygon, and let $\varepsilon > 0$ be smaller than half of any
 576 distance between two non-incident features of P . Then the ε -*chamfered* polygon \bar{P} is another
 577 polygon with twice as many vertices as P , defined as follows. Refer to Figure 22. For each
 578 vertex v_i of P , we create two new vertices v'_i and v''_i , where v'_i is placed on e_{i-1} at distance ε
 579 from v_i , and v''_i is placed on e_i at distance ε from v_i . Edge e'_i in \bar{P} connects v''_i to v'_{i+1} , and
 580 a new *short edge* s_i connects v'_i to v''_i . Note that the condition on ε implies that \bar{P} is itself a
 581 simple (i.e., not self-intersecting) polygon.

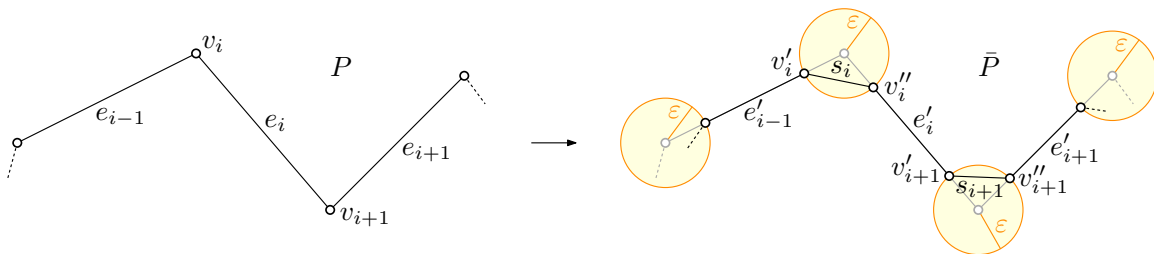


Figure 22: The chamfering operation.

582 The chamfering operation alters the local structure of the attraction diagram near
 583 every vertex. The idea is that at non-degenerate configurations, the change will not influence

584 the behavior of the puppy, and as such will not influence the existence of any catching
 585 strategies. However, at degenerate configurations, the change in the structure is significant.
 586 We will argue in Section 5.5 that the changes are such that every strategy in the chamfered
 587 polygon translates to a strategy in the original polygon.

588 Here we review again the different types of degenerate pivot configurations, and how
 589 the ε -chamfering operation, for a small-enough ε , affects the local structure of the attraction
 590 diagram in each case. Refer to Figure 23.

- 591 • Near type-1 degeneracies, the higher-degree vertices on the main diagonal disappear.
 592 Instead, two separate critical curves almost touch the main diagonal: one from above
 593 and one from below.
- 594 • Near type-2a degeneracies, the degree-4 vertex disappears. Instead, the two incident
 595 critical curves coming from the left are connected, and the two incident curves coming
 596 from the right are connected.
- 597 • Near type-2b degeneracies, the isolated pivot vertex simply disappears.
- 598 • Near type-3 degeneracies, the degenerate pivot “vertex” disappears. Any connected
 599 critical curve is locally rerouted away from the degenerate location.

600 5.5 Catching puppies on arbitrary simple polygons

601 Even when the chamfering radius ε is arbitrarily small, the attraction diagram of the chamfered
 602 polygon \bar{P} may have type-2b and type-3b degeneracies, and even new non-degenerate critical
 603 curves, that are not present in the original attraction diagram. See Figures 24 and 25 for
 604 examples. We argue in the next lemma that these are the only degeneracies that can appear
 605 in \bar{P} .

606 **Lemma 13.** *Let P be an arbitrary simple polygon. For all sufficiently small ε , the ε -chamfered*
 607 *polygon \bar{P} has no degenerate pivot configurations of type 1, type 2a, or type 3a.*

608 *Proof.* First, note that \bar{P} has no type-1 or type-3a degeneracies: we replace each vertex v_i with
 609 angle α_i by two new vertices v'_i and v''_i with angles $\alpha'_i = \alpha''_i = \pi - \frac{1}{2}(\pi - \alpha_i) = \frac{1}{2}\pi + \frac{1}{2}\alpha_i > \frac{1}{2}\pi$.

610 Next, we consider the type-2 degeneracies, which may occur for some values of ε . We
 611 argue that each potential type-2a degeneracy only occurs for at most one value of ε ; since
 612 there are finitely many potential degeneracies, the lemma then follows.

613 Note that, as we vary ε , all vertices of \bar{P} move linearly and with equal speed. Thus, if
 614 more than one value of ε gives rise to a type-2a degeneracy, then all of them do. There are two
 615 configurations in \bar{P} that could potentially give rise to infinitely many type-2a degeneracies.
 616 We argue that, in fact, such configurations cannot satisfy all requirements of a type-2a
 617 degeneracy.

- 618 • An edge e'_i has endpoint v'_i (or symmetrically, v''_{i-1}) such that the line ℓ through v'_i and
 619 perpendicular to e'_i contains another vertex v'_j (or v''_{j-1}). Refer to Figure 26. Then, as

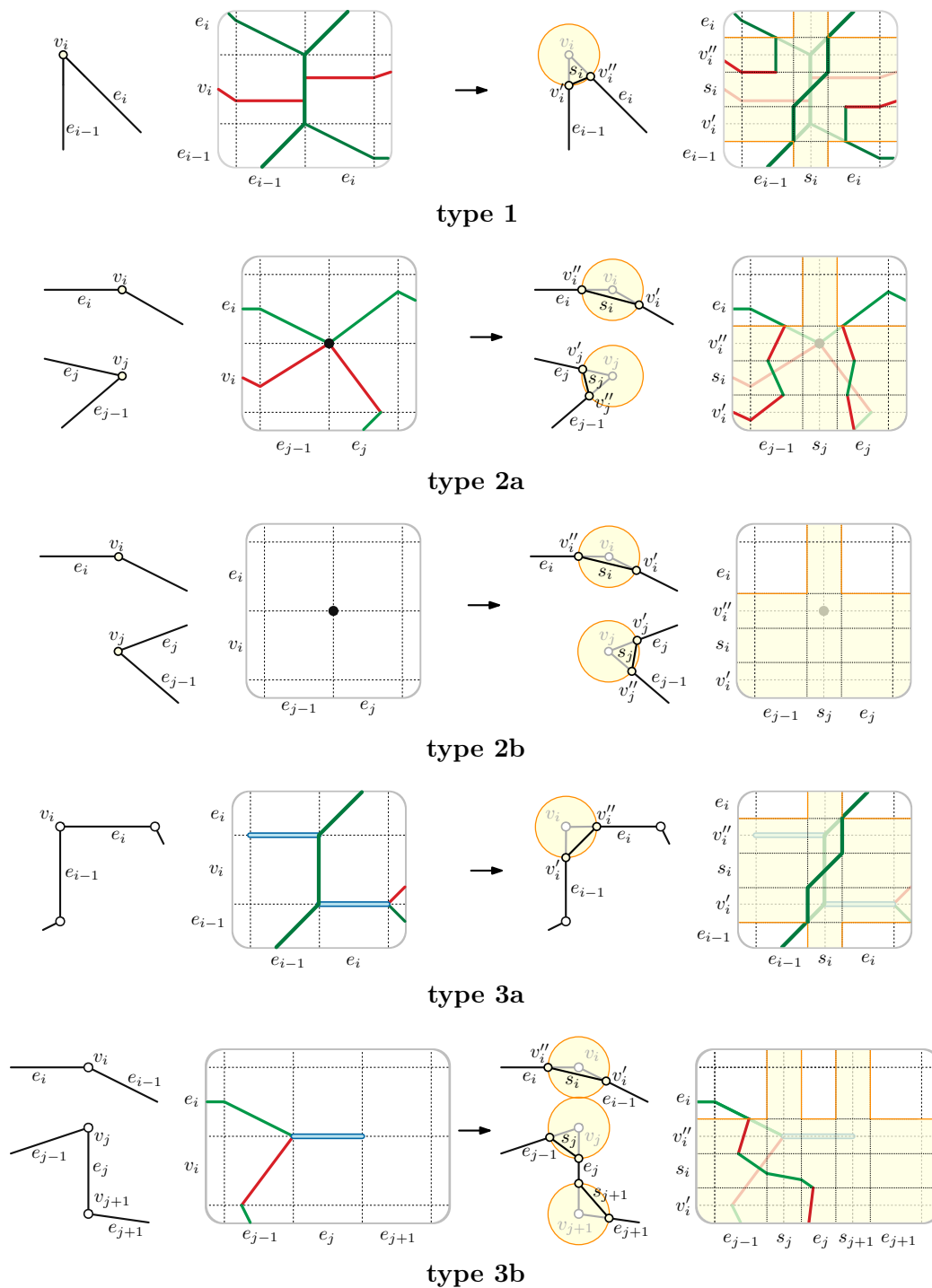


Figure 23: Effect of the chamfering operation on the attraction diagram near degenerate pivot configurations. The size of ε is exaggerated; the figures show the combinatorial structure of the chamfered diagram for a much smaller value of ε . Only the effect of chamfering vertices relevant for the degeneracy is shown.

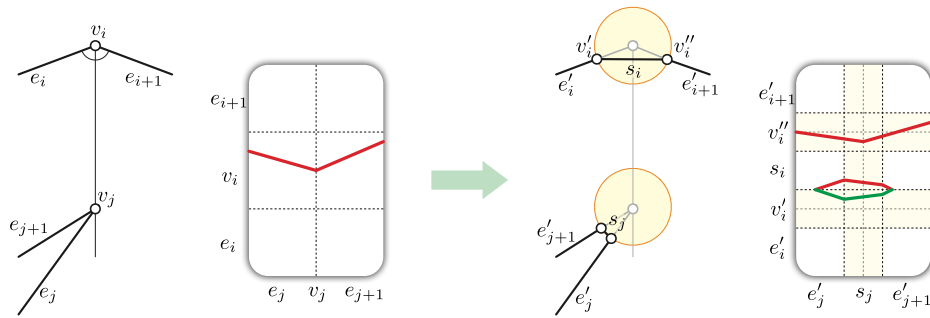


Figure 24: Chamfering P can create a new non-degenerate critical curve when one vertex of P lies on the angle bisector of another.

620 v'_i moves along e'_i , ℓ moves at the same speed as v'_i , and v'_j moves in the same direction
 621 at the same speed along e'_j . So e'_j is parallel to e'_i . But since the angles of \bar{P} are obtuse,
 622 we conclude that v''_{j-1} and v''_j lie on the opposite sides of ℓ ; thus, this cannot be a
 623 type-2 degeneracy.

- 624 • A short edge s_i of \bar{P} has an endpoint v'_i (or symmetrically, v''_i) such that the line ℓ
 625 through v'_i and perpendicular to s_i contains another vertex v'_j (or v''_{j-1}). Refer to
 626 Figure 27. In this case, vertex v_j must lie on the angle bisector of edges e_i and e_{i+1} ,
 627 and edges e_i and e_j must be parallel. Because the angles of \bar{P} are obtuse, s_i and e'_i
 628 lie on opposite sides of ℓ . Now, as ε varies, v'_i moves along e'_i , the slope of s_i does not
 629 change, and thus ℓ remains parallel to itself. Since v'_j moves in a direction concordant
 630 with ℓ 's direction, e'_j lies on the same sides of ℓ as e'_i . Thus, this cannot be a type-2a
 631 degeneracy. Note that it is possible that v''_j lies on the same side of ℓ as e'_j , in which
 632 case we have a degeneracy of type 2b (Figure 27 (left)), or that v''_j lies on ℓ , in which
 633 case we have a degeneracy of type 3b (Figure 27 (middle)). If v''_j lies on the opposite
 634 side of ℓ , there is no degeneracy (Figure 27 (right)). □

635 Note that it may be tempting to define a different chamfering parameter ε for each
 636 vertex of P , in order to eliminate also the type-2b and type-3b degeneracies from \bar{P} . The
 637 reason why we insist on having the same ε for all vertices will become apparent shortly, when
 638 proving Lemma 14.

639 Let P be an arbitrary simple polygon and \bar{P} an ε -chamfered copy without degeneracies
 640 of type 1, type 2a, or type 3a. We say a parameter value x is *verty* whenever $P(x)$ is at
 641 distance at most ε from a vertex of P . We say a parameter value x is *edgy* if it is not verty.
 642 We reparameterize \bar{P} such that $P(x) = \bar{P}(x)$ whenever x is edgy; the parameterization of \bar{P}
 643 is uniformly scaled for verty parameters. We say a configuration (x, y) is edgy when x and y
 644 are both edgy.

645 We say a path in the attraction diagram is *valid* if it describes a human and puppy
 646 behavior that obeys the rules imposed on the puppy and the human, as explained in Section 1.
 647 For polygonal tracks, it is not restrictive to assume that a valid path is piecewise linear, and
 648 that the derivative of the human's parameter value x only changes sign at pivot configurations
 649 (that is, the human may invert direction along the curve only when the configuration is a
 650 pivot one).

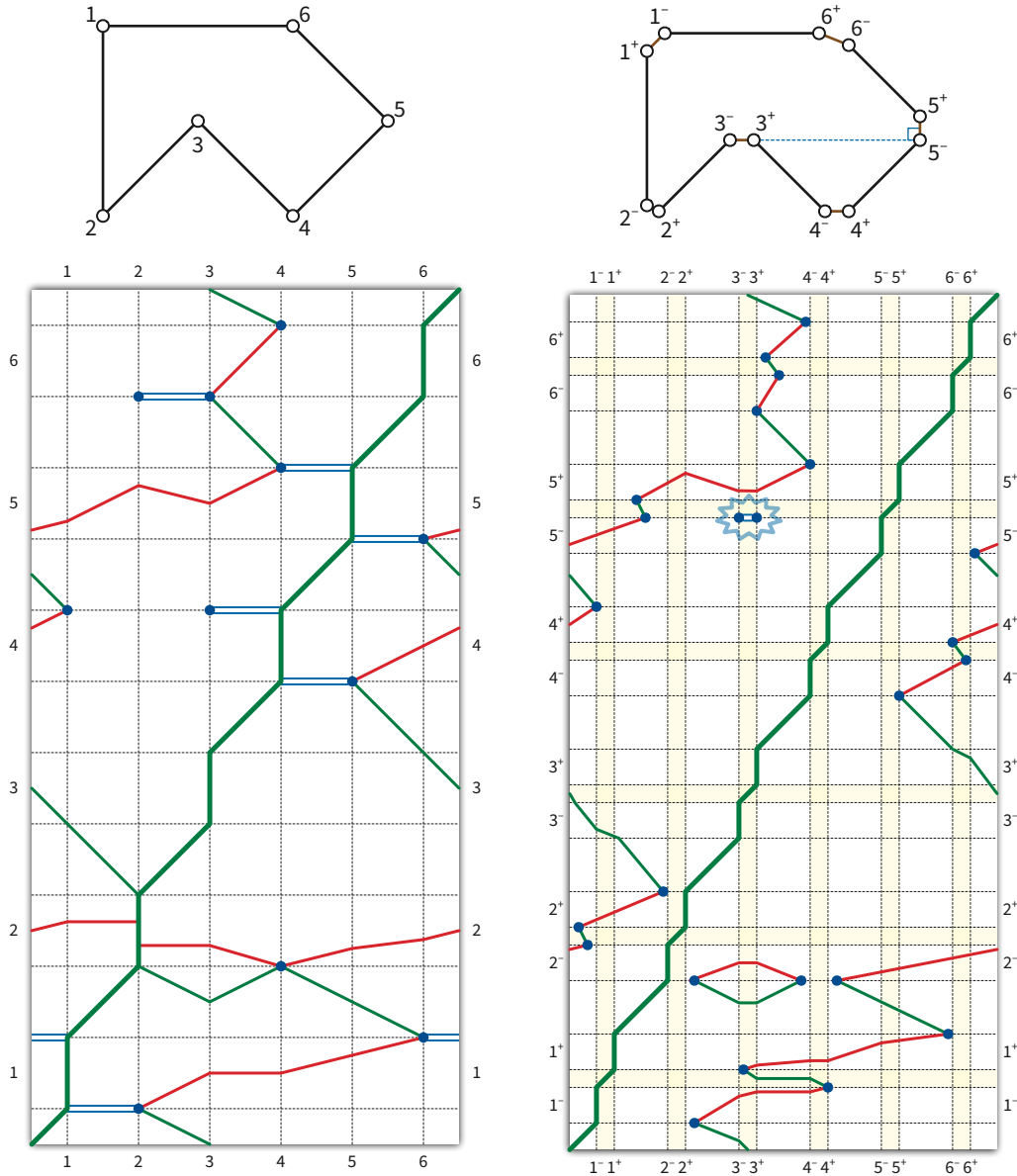


Figure 25: The attraction diagram of a degenerate polygon, before and after chamfering. All existing degeneracies disappeared in the chamfered polygon, which does have one new but harmless type-3b degeneracy.

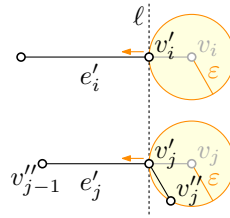


Figure 26: Potential new degenerate pivot configurations based on a (shortened) original edge e'_i . For ε small enough, there can be no degeneracy.

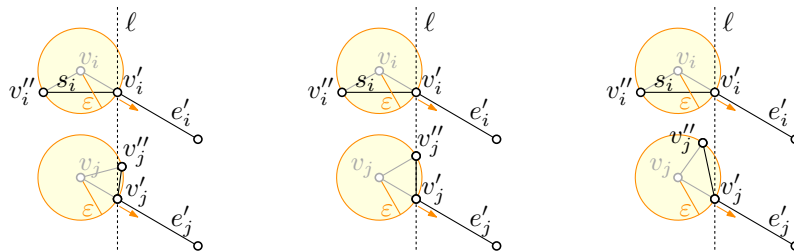


Figure 27: Potential new degenerate pivot configurations based on a short edge s_i . For any ε we may still have a new degeneracy of type 2b (left), 3b (middle), or no degeneracy (right).

651 **Lemma 14.** *Assuming ε is sufficiently small, for any valid path σ between two stable edge*
 652 *configurations (x_1, y_1) and (x_2, y_2) in the attraction diagram of \bar{P} , there is a valid path σ'*
 653 *between (x_1, y_1) and (x_2, y_2) in the attraction diagram of P .*

654 *Proof.* We will describe how to obtain σ' by slightly deforming σ in the non-edge confi-
 655 gurations, assuming that ε is small enough. In fact, it will suffice to show that σ and σ'
 656 determine the same “qualitative behavior” of the puppy. That is, let ψ be a valid path in
 657 the attraction diagram of P or \bar{P} , and consider the ordered sequence of all configurations
 658 $((\tilde{x}_i, \tilde{y}_i))_{1 \leq i \leq k}$ along ψ where the puppy’s parameter value \tilde{y}_i transitions from edge to vertex or
 659 vice versa. The *qualitative behavior* of the puppy determined by ψ is defined as the sequence
 660 $q_\psi = (\tilde{y}_i)_{1 \leq i \leq k}$. We will show that $q_\sigma = q_{\sigma'}$, thus proving the lemma.

661 The intuition is that there is a direct correspondence between edge configurations
 662 in the two diagrams, and we only have to ensure that the puppy has the correct behavior
 663 when the configuration is not edgey, i.e., the human or the puppy is in an ε -neighborhood of
 664 a vertex of P .

665 Let ρ be a maximal subpath of σ where the puppy’s parameter y remains edgey except
 666 possibly at the endpoints, i.e., the puppy remains on some edge e'_i of \bar{P} while the human walks
 667 along \bar{P} . We argue that, if the human moves in the same way along P , thus determining
 668 a path ρ' in the attraction diagram of P , then the puppy never leaves e_i . Moreover, if ρ
 669 terminates with the puppy on an endpoint of e'_i , say v''_i , then ρ' terminates with the puppy
 670 in a vertex position corresponding to v_i .

671 Observe that, if the projection of a vertex v_j on the line supporting e_i lies in the
 672 interior of e_i , then the projection of the short edge s_j on the same line lies in the interior of

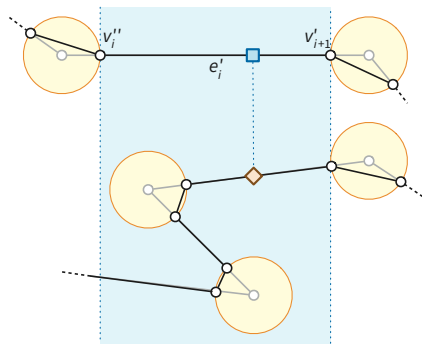


Figure 28: As long as the puppy stays on the chamfered edge e'_i , its qualitative behavior is the same on the original and chamfered polygon.

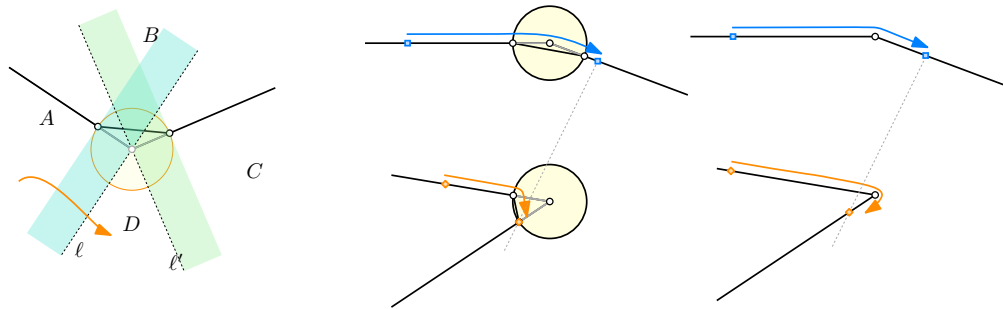


Figure 29: Left: When the puppy is around a vertex, its qualitative behavior is determined by the region where the human lies (either A , B , C , or D). Center and right: Once the human gets in a neighborhood of the lower vertex, the puppy makes a jump forward. This behavior can be replicated in P , as the configuration corresponds to a type-2a degeneracy.

673 e'_i , assuming that ε is small enough. Thus, the puppy's behavior according to ρ' is the same
 674 as with ρ , except when the human reaches a neighborhood of a vertex v_j that projects on an
 675 endpoint of e_i , say v_i .

676 In the latter case, since the chamfering parameter ε is the same for both v_i and v_j ,
 677 the human cannot reach the interior of the short edge s_j before the puppy reaches the interior
 678 of the short edge s_i . However, since ρ keeps the puppy on e'_i , this is not possible. Thus, the
 679 puppy in ρ' behaves in the same way as in ρ in every case. See Figure 28.

680 Let us now consider a maximal subpath τ of σ where the puppy's parameter y
 681 remains verty. Furthermore, assume that both endpoints of τ have a puppy parameter at
 682 the boundary between verty and edgy (such is the situation when τ is between two subpaths
 683 of σ where the puppy parameter is edgy). As before, we will construct a path τ' in the
 684 attraction diagram of P such that the puppy has the same qualitative behavior as in τ . Refer
 685 to Figure 29.

686 By assumption, throughout τ , the puppy always remains on a short edge, say s_i ,
 687 possibly rotating its direction vector while it is at a vertex of s_i . Let ℓ and ℓ' be the lines
 688 through v_i orthogonal to e_{i-1} and e_i , respectively. We say that v_i is *generic* if no other

689 vertex lies on either ℓ or ℓ' . We denote by S the infinite strip of width ε bounded by ℓ and
 690 v'_i . Similarly, we denote the infinite strip bounded by ℓ' and v''_i by S' .

691 If v_i is generic, then we can choose ε small enough such that the strips S and S'
 692 intersect no short edges of \bar{P} other than s_i . Thus, whenever the human moves within one
 693 of the strips S or S' , it stays within some edge e'_j of \bar{P} . It follows that, if the human in τ'
 694 replicates the identical behavior within S and S' as the human in τ , this determines the same
 695 qualitative behavior of the puppy (i.e., the puppy in τ leaves s_i from one of its endpoints if
 696 and only if the puppy in τ' moves to the corresponding edgy position in P).

697 Denote by A, B, C, D the four regions of the plane bounded by ℓ and ℓ' , as in
 698 Figure 29 (left), and assume that the human in τ moves outside of S and S' within one
 699 of these four regions. In the case of D , the puppy never leaves s_i ; replicating the human's
 700 movements in P (straightforwardly modified around the vertices to match the shape of P)
 701 causes the puppy to stay at v_i , thus having the same qualitative behavior. On the other
 702 hand, if the human is anywhere in $A \setminus S$ or in $C \setminus S'$, the puppy immediately moves to an
 703 edgy position, both in \bar{P} and in P .

704 Suppose now that the human is in B , and consider the open strip S'' consisting of
 705 the union of all the lines perpendicular to s_i that intersect the interior of s_i . If the human
 706 moves within $B \setminus (S \cup S' \cup S'')$, we reason in the same way as with $A \setminus S$ and $C \setminus S'$. If
 707 the human is anywhere in $B \cap S''$, then the configuration stabilizes with the puppy in the
 708 interior of s_i . However, observe that, in order to reach this region, the human must have
 709 crossed $B \cap S''$, thus causing the puppy to move outside of s_i or never enter s_i in the first
 710 place. Hence, this case never occurs.

711 Finally, let us consider the case where v_i is not generic. We can argue in the same
 712 way as in the generic case, except when the human moves in a neighborhood of a vertex v_j
 713 that lies on, say, ℓ . In this case, we can choose ε small enough so that both S' and S'' (as
 714 defined above) are disjoint from the disk of radius ε centered at v_j . Now, if the human ever
 715 enters the region C while in a neighborhood of v_j , we can reason as above.

716 The only remaining case is the one where v_i and v_j give rise to a type-2a degeneracy
 717 in the attraction diagram of P , as illustrated in Figure 29 (center and right). Since the
 718 chamfering parameter ε is the same for both v_i and v_j , the short segment s_j lies entirely in
 719 the strip S . Also, by our choice of ε , s_j lies outside the open strip S'' . Thus, if the human in
 720 τ ever reaches s_j , the puppy exits s_i from v''_i . This behavior can be replicated in P if the
 721 human moves to the vertex v_j , which causes the puppy to travel around vertex v_i .

722 We have proved that the path σ can be decomposed into subpaths $\rho_1, \tau_1, \rho_2, \tau_2,$
 723 \dots, ρ_k , each of which has a corresponding path ρ'_i or τ'_i in the attraction diagram of P
 724 which determines the same qualitative behavior of the puppy. By definition of "qualitative
 725 behavior", the ending point of any path in the sequence $\rho'_1, \tau'_1, \rho'_2, \tau'_2, \dots, \rho'_k$ coincides with
 726 the starting point of the next path. Thus, the paths can be concatenated to form the desired
 727 path σ' . □

728 We are now ready to prove our main result.

729 **Theorem 15.** *Let P be a simple polygon. The human can catch the puppy on P , starting*
 730 *from any initial configuration.*

731 *Proof.* Let ε be so small as to satisfy both Lemma 13 and Lemma 14. Consider an arbitrary
732 starting configuration on P . If the starting configuration is not stable, we let the puppy
733 move until it is. If the resulting configuration is not edgy, we move the human along P until
734 we reach an edgy configuration (x, y) . (This must be possible, except if the puppy stays
735 in an ε -neighborhood of a vertex for the entire time; in that case, we can catch the puppy
736 trivially, by going to that vertex.)

737 By Lemma 13, the ε -chamfered polygon \bar{P} has no degeneracies of type 1 or type 2a or
738 type 3a. Thus, by Corollary 12, there exists a strategy for the human to catch the puppy on
739 \bar{P} . If the end configuration of this strategy is not edgy, we may now simply move human and
740 puppy together to an edgy final configuration (f, f) . By Lemma 14, there is an equivalent
741 strategy to reach (f, f) from (x, y) on P . Combined with the initial path to (x, y) , this gives
742 us a path from an arbitrary starting configuration to a final configuration on P . \square

743 6 Further questions

744 For simple curves, we have only proved that a catching strategy exists. At least for polygonal
745 tracks, it is straightforward to compute such a strategy in $O(n^2)$ time by searching the
746 attraction diagram. In fact, we can compute a strategy that minimizes the total distance
747 traveled by either the human or the puppy in $O(n^2)$ time, using fast algorithms for shortest
748 paths in toroidal graphs [15, 17]. Unfortunately, this quadratic bound is tight in the worst
749 case if the output strategy must be represented as an explicit path through the attraction
750 diagram. We conjecture that an optimal strategy can be described in only $O(n)$ space
751 by listing only the human's initial direction and the sequence of points where the human
752 reverses direction. On the other hand, an algorithm to compute such an optimal strategy in
753 subquadratic time seems unlikely.

754 If the track is a *smooth curve* of length ℓ whose attraction diagram has k pivot
755 configurations, a trivial upper bound on the distance the human must walk to catch the
756 puppy is $\ell \cdot k/2$. In any optimal strategy, the human walks straight to the point on the curve
757 corresponding to a pivot located at one of the two endpoints of the current "stable sub-curve"
758 of a critical curve (walking less than ℓ). Then the configuration moves to another stable
759 sub-curve, and so on, never visiting the same stable sub-curve twice. Our question is whether
760 a better upper bound can be proved.

761 In fact, if minimizing distance is not a concern, we conjecture that *no* reversals are
762 necessary. That is, on *any* simple track, starting from *any* configuration, we conjecture that
763 the human can catch the puppy *either* by walking only forward along the track *or* by walking
764 only backward along the track. Figure 2 and its reflection show examples where each of these
765 naïve strategies fails, but we have no examples where both fail. (Our proof of Theorem 2
766 implies that the human can always catch the puppy on an *orthogonal* polygon by walking *at*
767 *most once* around the track in some direction, depending on the starting configuration.)

768 More ambitiously, we conjecture that the following *oblivious* strategy is always
769 successful: walk twice around the track in one (arbitrary) direction, then walk twice around
770 the track in the opposite direction.

771 Another interesting question is to what extent our result applies to self-intersecting
772 curves in the plane, when we consider the two strands of the curve at an intersection point to
773 be distinct. It is easy to see that the human cannot catch the puppy on a curve that traverses
774 a circle twice; see Figure 4. Indeed, we know how to construct examples of bad curves with
775 any rotation number *except* -1 and $+1$. We conjecture that Lemma 5, and therefore our
776 main result, extends to all non-simple tracks with rotation number ± 1 . Similarly, are there
777 interesting families of curves in \mathbb{R}^3 there the human and puppy can always meet?

778 Finally, it is natural to consider similar pursuit-attraction problems in more general
779 domains. Theorem 1 shows that the human can always catch the puppy in the interior of a
780 simple polygon, by walking along the dual tree of any triangulation. Can the human always
781 catch the puppy in any planar straight-line graph? Inside any polygon with holes?

782 Acknowledgements

783 The authors would like to thank Ivor van der Hoog, Marc van Kreveld, and Frank Staals for
784 helpful discussions in the early stages of this work, and Joseph O'Rourke for clarifying the
785 history of the problem. Portions of this work were done while the second author was visiting
786 Utrecht University.

787 M.A. partially supported by the VILLUM Foundation grant 16582. M.L. partially
788 supported by the Dutch Research Council (NWO) under project number 614.001.504 and
789 628.011.005. T.M. supported by the Dutch Research Council (NWO) under Veni grant
790 EAGER J.U. supported by the Dutch Research Council (NWO) under project number
791 612.001.651. J.V. supported by the Dutch Research Council (NWO) under project number
792 612.001.651.

793 References

- 794 [1] Zachary Abel, Hugo A. Akitaya, Erik D. Demaine, Martin L. Demaine, Adam Hesterberg,
795 Matias Korman, Jason S. Ku, and Jayson Lynch. Negative instance for the edge patrolling
796 beacon problem. *Preprint*, <https://arxiv.org/abs/2006.01202>, 2020.
- 797 [2] Israel Aldana-Galván, Jose L. Alvarez-Rebollar, Juan Carlos Cataa-Salazar, Nestaly
798 Marin-Nevárez, Erick Solís-Villareal, Jorge Urrutia, and Carlos Velarde. Beacon cov-
799 erage in orthogonal polyhedra. In *Proceedings of the 29th Canadian Conference on*
800 *Computational Geometry (CCCG 2017)*, pages 156–161, 2017.
- 801 [3] Israel Aldana-Galván, Jose L. Alvarez-Rebollar, Juan Carlos Cataa-Salazar, Nestaly
802 Marin-Nevárez, Erick Solís-Villareal, Jorge Urrutia, and Carlos Velarde. Tight bounds
803 for illuminating and covering of orthotrees with vertex lights and vertex beacons. *Graphs*
804 *and Combinatorics*, 36:617–630, 2929.
- 805 [4] Helmut Alt and Michael Godau. Computing the Fréchet distance between two polygonal
806 curves. *Int. J. Comput. Geom. Appl.*, 5:75–91, 1995. doi:10.1142/S0218195995000064.

- 807 [5] Sang Won Bae, Chan-Su Shin, and Antoine Vigneron. Tight bounds for beacon-based
808 coverage in simple rectilinear polygons. *Computational Geometry*, 80:40–52, 2019.
809 [doi:10.1016/j.comgeo.2019.02.002](https://doi.org/10.1016/j.comgeo.2019.02.002).
- 810 [6] Michael Biro. *Beacon-based routing and guarding*. PhD thesis, State University of New
811 York at Stony Brook, 2013.
- 812 [7] Michael Biro, Jie Gao, Justin Iwerks, Irina Kostitsyna, and Joseph S. B. Mitchell. Beacon-
813 based routing and coverage. In *Proceedings of the 21st Fall Workshop on Computational
814 Geometry*, 2011.
- 815 [8] Michael Biro, Jie Gao, Justin Iwerks, Irina Kostitsyna, and Joseph S. B. Mitchell.
816 Beacon based structures in polygonal domains. In *Abstracts of the 1st Computa- tional
817 Geometry: Young Researchers Forum*, 2012.
- 818 [9] Michael Biro, Jie Gao, Justin Iwerks, Irina Kostitsyna, and Joseph S. B. Mitchell.
819 Combinatorics of beacon routing and coverage. In *Proceedings of the 25th Canadian
820 Conference on Computational Geometry (CCCG 2013)*, 2013.
- 821 [10] Michael Biro, Justin Iwerks, Irina Kostitsyna, and Joseph S. B. Mitchell. Beacon-based al-
822 gorithms for geometric routing. In *13th International Symposium on Algorithms and Data
823 Structures (WADS 2013)*, pages 158–169, 2013. [doi:10.1007/978-3-642-40104-6_14](https://doi.org/10.1007/978-3-642-40104-6_14).
- 824 [11] Prosenjit Bose and Thomas C. Shermer. Gathering by repulsion. *Computational
825 Geometry*, 90:101627, 2020. [doi:10.1016/j.comgeo.2020.101627](https://doi.org/10.1016/j.comgeo.2020.101627).
- 826 [12] Pierre Bouguer. Sur de nouvelles courbes ausquelle on peut donner le nom de linges de
827 poursuite. *Mémoires de mathématique et de physique tirés des registres de l'Académie
828 royale des sciences*, pages 1–14, 1732. URL: [https://gallica.bnf.fr/ark:/12148/
829 bpt6k35294](https://gallica.bnf.fr/ark:/12148/bpt6k35294).
- 830 [13] Johans Cleve and Wolfgang Mulzer. Combinatorics of beacon-based routing in three
831 dimensions. *Computational Geometry*, 91:101667, 2020. [doi:10.1016/j.comgeo.2020.
832 101667](https://doi.org/10.1016/j.comgeo.2020.101667).
- 833 [14] Pierre de Maupertuis. Sure les courbes de poursuite. *Mémoires de mathématique et de
834 physique tirés des registres de l'Académie royale des sciences*, pages 15–17, 1732. URL:
835 <https://gallica.bnf.fr/ark:/12148/bpt6k35294>.
- 836 [15] John R. Gilbert, Joan P. Hutchinson, and Robert Endre Tarjan. A separator
837 theorem for graphs of bounded genus. *J. Algorithms*, 5(3):391–407, 1984. [doi:
838 10.1016/0196-6774\(84\)90019-1](https://doi.org/10.1016/0196-6774(84)90019-1).
- 839 [16] Arthur S. Hathaway. Problems and solutions: Problem 2801. *American Mathematical
840 Monthly*, 27(1):31, 1920. [doi:10.2307/2973244](https://doi.org/10.2307/2973244).
- 841 [17] Monika R. Henzinger, Philip Klein, Satish Rao, and Sairam Subramanian. Faster
842 shortest-path algorithms for planar graphs. *J. Comput. Syst. Sci.*, 55(1):3–23, 1997.
843 [doi:10.1006/jcss.1997.1493](https://doi.org/10.1006/jcss.1997.1493).

- 844 [18] Irina Kostitsyna, Bahram Kouhestani, Stefan Langerman, and David Rappaport. An
845 Optimal Algorithm to Compute the Inverse Beacon Attraction Region. In *34th*
846 *International Symposium on Computational Geometry (SoCG 2018)*, 2018. doi:
847 [10.4230/LIPIcs.SocG.2018.55](https://doi.org/10.4230/LIPIcs.SocG.2018.55).
- 848 [19] Bahram Kouhestani and David Rappaport. Edge patrolling beacon. In *Abstracts from*
849 *the 20th Japan Conference on Discrete and Computational Geometry, Graphs, and*
850 *Games (JCDCGGG 2017)*, pages 101–102, 2017.
- 851 [20] Bahram Kouhestani, David Rappaport, and Kai Salomaa. On the inverse beacon
852 attraction region of a point. In *Proceedings of the 27th Canadian Conference on*
853 *Computational Geometry (CCCG 2015)*, 2015.
- 854 [21] Bahram Kouhestani, David Rappaport, and Kai Salomaa. The length of the beacon
855 attraction trajectory. In *Proceedings of the 28th Canadian Conference on Computational*
856 *Geometry (CCCG 2016)*, pages 69–74, 2016.
- 857 [22] Bahram Kouhestani, David Rappaport, and Kai Salomaa. Routing in a polygonal
858 terrain with the shortest beacon watchtower. *Computational Geometry*, 68:34–47, 2018.
859 doi:[10.1016/j.comgeo.2017.05.005](https://doi.org/10.1016/j.comgeo.2017.05.005).
- 860 [23] John E. Littlewood. *Littlewood’s Miscellany: edited by Béla Bollobás*. Cambridge
861 University Press, 1986.
- 862 [24] Amirhossein Mozafari and Thomas C. Shermer. Transmitting particles in a polygonal do-
863 main by repulsion. In *12th International Conference on Combinatorial Optimization and*
864 *Applications (COCOA 2018)*, pages 495–508, 2018. doi:[10.1007/978-3-030-04651-4_](https://doi.org/10.1007/978-3-030-04651-4_33)
865 [33](https://doi.org/10.1007/978-3-030-04651-4_33).
- 866 [25] Paul J. Nahin. *Chases and Escapes: The Mathematics of Pursuit and Evasion*. Princeton
867 University Press, 2007.
- 868 [26] Thomas C. Shermer. A combinatorial bound for beacon-based routing in orthogonal
869 polygons. In *Proceedings of the 27th Canadian Conference on Computational Geometry*
870 *(CCCG 2015)*, 2015.